Contract No:

This document was prepared in conjunction with work accomplished under Contract No. DE-AC09-08SR22470 with the U.S. Department of Energy (DOE) Office of Environmental Management (EM).

Disclaimer:

Hanford Double Shell Waste Tank Corrosion Studies – Final Report FY2018

R. E. Fuentes

P. K. Shukla

B. Peters

D. A. Hitchcock

August 2019

SRNL-STI-2019-00014, Revision 0

DISCLAIMER

Printed in the United States of America

Prepared for
U.S. Department of Energy

SRNL-STI-2019-00014
Revision 0

Keywords: *Hanford, Chemistry Control, Vapor Corrosion Inhibitor, Ammonia Sensor*

Retention: *Permanent*

HANFORD DOUBLE SHELL WASTE TANK CORROSION STUDIES – FINAL REPORT FY2018

R. E. Fuentes
P. K. Shukla
B. Peters
D. A. Hitchcock

August 2019

Prepared for the U.S. Department of Energy under contract number DE-AC09-08SR22470.

Savannah River National Laboratory™
OPERATED BY SAVANNAH RIVER NUCLEAR SOLUTIONS

REVIEWS AND APPROVALS

AUTHORS:

R. E. Fuentes, Materials Science and Technology Date

P. K. Shukla, Materials Science and Technology Date

B. Peters, Energy Materials Programs Date

D. A. Hitchcock, Energy Materials Programs Date

TECHNICAL REVIEW:

J. T. Boerstler, Materials Science and Technology, Review per E7 2.60 Date

APPROVAL:

B. J. Wiersma, Manager Date
Corrosion and Materials Performance, Materials Science and Technology

C. L. Girardot, Manager Date
Washington River Protection Solutions

J. Castleberry, Manager Date
Washington River Protection Solutions

ACKNOWLEDGEMENTS

The efforts of T. Murphy, B. Hill and S. Crossland are greatly appreciated in providing technical support for performing experiments and characterizations. Helpful consultations and recommendations from L. Stock and WRPS Corrosion Sub-group provided guidance for the achievement of tasks. Additionally, the authors acknowledge the assistance of S. P. Harris for providing statistical modeling and analysis for the New Limits Task.

EXECUTIVE SUMMARY

For FY18, Savannah River National Laboratory (SRNL) focused on four main tasks in its study of corrosion of Hanford Double-Shell Tanks (DSTs). The New Limits task focused on the development of a pitting factor as a localized corrosion predictor. Electrochemical experiments were directed towards pitting factors between 1 and 2 (i.e., borderline conditions) and separating the effects of chloride and fluoride in the pitting factor equation. In addition, long term immersion testing experiments with partial and completely immersed coupons in solutions with a wide range of pitting factors were tested. Secondary liner studies continued this year with a new vapor corrosion inhibition (VCI) strategy in which ground water (GW) simulants at a specified concentration of commercial VCI were mixed. The specific concentrations were recommended by Cortec® and was compared with similar concentration of GW with calcium carbonate. The anodic drift task utilized a simulant corresponding to AN-107 waste tank chemistry. The chemistry was studied with three different surface conditions: mill-scale, partial mill-scale and ground to 600 grit to study the impact of different surfaces on the potential drift. The final task was focused on ammonia concentration determination of a vapor space corrosion (VSC) test vessel using Quartz-Enhanced Photoacoustic Spectroscopy (QEPAS) detector. A summary of each task is presented below.

1. New Limits

Immersion tests were performed using simulants with a wide range of pitting factors. A coupon in each test was partially immersed to identify liquid-air interface (LAI) and vapor space (VS) corrosion, and another was completely immersed connected electrically to obtain open circuit potential (OCP) measurements to identify corrosion activity and susceptibility. For the immersion tests, severe LAI corrosion was observed in three cases where the pitting factor was less than 0.5. Mitigation of LAI corrosion requires that the hydroxide concentration be maintained greater than 0.01 M and the pitting factor greater than 1.2.

Electrochemical testing in FY18, focused on pitting factors between 1 to 2 to target corrosion susceptibility for established borderline conditions and on fluoride effects to separate the halide coefficient in the pitting factor equation for fluoride and chloride contributions. Fifteen tests with duplicates were performed with pitting factors 1 to 2 and slightly above and it was observed that nine of the thirty runs showed mixed hysteresis. After running modified ASTM G192 tests, most of the tests showed a passing category with just one fail. Even though, the use of a modified ASTM G192 test was needed for determination of pass or fail, it seems that for pitting factors higher than 1, a pass is the most likely response with a greater than 90% success rate for the 15 tests performed. A round of fifteen tests with no duplicate runs were tested to determine the effect of fluoride. Logistic regression was performed with the results of pitting factor between 1 and 2 and fluoride effects. The contribution of chloride for the equation is around 3 times more significant than fluoride.

The pitting factor equation obtained was used to establish new corrosion control limits recommended for DSTs. The equation was validated with model simulations and comparison with historical results. The results were compiled in a memorandum that was submitted to WRPS summarizing the technical basis for the recommended changes in the chemistry controls. The resulting equation obtained is presented below,

$$\text{Pitting Factor} = \frac{\text{Inhibitor Species}}{\text{Aggressive Species}} = \frac{8.06\,[\text{OH-}] + 1.55\,[\text{NO}_2\text{-}]}{[\text{NO}_3\text{-}] + 16.7\,[\text{Cl-}] + 5.7\,[\text{Fl-}]}$$

2. Secondary Liner Corrosion Tests

Vapor Space Corrosion (VSC) and immersion tests with commercially available vapor corrosion inhibitors (VCIs) were performed on rail-road car carbon steel samples at specific concentrations mixed with the groundwater simulant that has been pH adjusted to alkaline conditions. VCIs used for the study included:

- VpCI-645 + VpCI-609 solution with 10% VpCI-609 by weight of solution (100 g VpCI-609 in 1 liter) and 0.75% VpCI-645 by volume (7.5 mL/L), and
- VpCI-337 – 10% solution, i.e., 100 mL in VpCI-337 plus 900 mL of water for 1 L of the VCI solution

The VCIs were directly added to the groundwater solution at the start of the tests. The carbon steel coupons were immersed in the solution and, also, suspended in the vapor space of the corrosion cells. The study results indicated that both VCIs, i.e., VpCI-645 + VpCI-609 and VpCI-337, are effective in mitigating corrosion. However, one vapor space coupon in VpCI-337 environment exhibited pitting corrosion, but none in VpCI-645 + VpCI-609. This suggest that VpCI-645 + VpCI-609 combination is slightly more effective than VpCI-337 alone in mitigating corrosion, although more tests are needed to confirm.

3. Anodic Drift

Anodic drift experimental studies were conducted using AN-107 simulant and rail-road car steel coupons. The focus of the study was to determine the effect of surface condition on OCP shift. AN-107 simulant was selected because pitting factor for the simulant was 1.66, which indicated uncertainty about the pitting corrosion tendency of the carbon steel. The study results showed that the drift could either be anodic or cathodic depending on the surface condition. For example, drift in corrosion potential was cathodic for the surface covered with mill-scale plus corrosion products, whereas the drift was anodic for an electrode with 600 grit ground surface. However, the terminal OCP values, i.e., OCP values at the steady-state were independent of the surface conditions. CPP data collected after OCP hold for 4 months indicated that pitting corrosion related electrochemical characteristics were not affected by the OCP evolution.

4. QEPAS studies

QEPAS was used to monitor the vapor space of a VSC test. Prior to configuring the system for this test, a new sensor was procured from Achray Photonics Inc. and several calibrations and tests were completed to confirm that the sensor was operational. These tests included: dry ammonia gas calibration at varying concentrations; testing to verify that moderate fluctuations in humidity would not affect the QEPAS sensor during operation; and an empty VSC vessel test. The humidity testing indicated that there was no significant change in the error within the system for ammonia concentrations below 250 ppm (~5% error) and only a slight increase was detected for concentrations above 250 ppm (~9% error). During the empty vessel VSC testing, residence times of more than 100 hours were observed, which indicate that a solution containing a source of ammonia is required for vapor space simulations. Lastly, simulant VSC testing was conducted using the same vessel that was used during the empty vessel testing. These results indicate that there is significant contribution from the solution to the ammonia present in the system, and that utilizing an ammonium nitrate-based solution reduces the residence time of the vessel from >100 hours to <1 hour.

TABLE OF CONTENTS

LIST OF TABLES

LIST OF FIGURES

LIST OF ABBREVIATIONS

ADS	Acoustic Detection Module
ASTM	American Society for Testing and Materials
CPP	Cyclic Potentiodynamic Polarization
DI	Deionized
DNV-GL	Det Norske Veritas-Germanischer Lloyd
DST	Double-Shell Tank
EDM	Electrical Discharge Machine
ER	Electrical Resistance
FY	Fiscal year
GW	Ground Water
LAI	Liquid-Air Interface
LDP	Leak Detection Pit
mpy	Mils per year
OCP	Open Circuit Potential
PP	polypropylene
PTFE	Polytetrafluoroethylene
QEPAS	Quartz-enhanced Photoacoustic Spectroscopy
QTF	Quartz Tuning Fork
SCC	Stress Corrosion Cracking
sccm	Standard cubic centimeter
SCE	Saturated Calomel Electrode
SRNL	Savannah River National Laboratory
SRS	Savannah River Site
SST	Single-Shell Tank
TAPI	Tank and Pipeline Integrity
TIC	Total Inorganic Carbon
TIEP-CSG	Tank Integrity Expert Panel-Corrosion Sub-Group
VCI	Vapor Corrosion Inhibitor
VS	Vapor Space
VSC	Vapor Space Corrosion
WRPS	Washington River Protection Solutions

1.0 Introduction

Single-shell tanks (SSTs) and double-shell tanks (DSTs) at Hanford Site are storing millions of gallons of radioactive waste. The tanks were fabricated of carbon steel and the liquid waste is pending stabilization into an immobilized waste form for permanent storage. A comprehensive chemical control program to maintain tank integrity until a disposition path is obtained is currently in place. The program is overseen by the Tank and Pipeline Integrity (TAPI) group from Washington River Protection Solutions (WRPS).

The liquid waste is currently being inhibited by maintaining alkaline conditions in the tank since carbon steel can undergo passive dissolution. Nonetheless, certain corrosive species in the waste chemistries, such as nitrate and chloride, could cause localized corrosion. For this reason and others, the chemical control program is continuously being updated for preventing susceptibility to stress corrosion cracking (SCC) and pitting corrosion.

Corrosion testing has been directed by the Tank Integrity Expert Panel-Corrosion Sub-Group (TIEP-CSG) to provide the technical guidelines for the corrosion control program. Testing for corrosion has been performed at three independent laboratories: Det Norske Veritas-Germanischer Lloyd (DNV-GL), Savannah River National Laboratory (SRNL), and the 222-S facility at Hanford operated by WRPS. SRNL has focused its corrosion studies on vapor space corrosion (VSC), development of corrosion chemistry limits to mitigate pitting corrosion, and corrosion protection for the tank secondary liner in DSTs.

Throughout fiscal year (FY) 2018, SRNL emphasized four primary activities for DSTs corrosion testing. Task one focused on new limits immersion testing and electrochemical testing to validate the pitting factor and to expand halides into the specific aggressiveness of chloride and fluoride. Electrochemical testing also was used to test conditions at pitting factors between 1 and 2 (i.e., borderline conditions) using simple chemistries with statistically significant species, and simulants based on tank chemistries. Task two was related to VSC studies for secondary liner to study vapor corrosion inhibition (VCI) practices using: commercial formulations and sodium carbonate as an inhibitor that can be present in concrete. The third task was an examination of anodic drift to test different material surfaces with a simulant and study the effects of surface on Open Circuit Potential (OCP) drift. Finally, the fourth task was the optimization of the Quartz-Enhanced Photoacoustic Spectroscopy (QEPAS) sensor for the detection of low levels of ammonia and testing in the VSC setup.

2.0 Background

FY18 Task Plan for the work to be performed for DSTs corrosion testing entailed four main tasks [1]. New Limits work was prioritized involving immersion testing and additional electrochemical testing. Long-term testing was performed for VSC corrosion using VCIs and starting of anodic drift studies. QEPAS analysis was added to include testing in the VSC setup. However, microbiologically induced corrosion studies were not carried out for this year. The four tasks for FY18 are numbered below with details about the objective of testing and background.

2.1 New Limits Corrosion Studies

The chemical control program at Hanford uses sodium hydroxide to maintain alkaline conditions and relies of radiolysis reactions that can turn the aggressive species nitrate into the inhibitor nitrite. Table 2-1 shows the current control program for Hanford DSTs [2] and illustrates the nitrate ranges and temperatures that needed to be maintained to control corrosion inside the tanks. Currently, all DST supernates are above 0.01 M hydroxide, satisfying the current corrosion control program requirement.

Table 2-1 Double-Shell Tank Waste Chemistry Limits for Corrosion Control

For $[NO_3^-]$ Range	Variable	For Waste Temperature (T) Range		
		T < 167 °F (75 °C)	167 °F (75 °C) ≤ T ≤ 212 °F (100 °C)	T > 212 °F (100 °C)
$[NO_3^-] \leq 1.0$ M	$[OH^-]$	0.010 M ≤ $[OH^-]$ ≤ 8. 0 M	0.010 M ≤ $[OH^-]$ ≤ 5.0 M	0.010 M ≤ $[OH^-]$ ≤ 4.0 M
	$[NO_2^-]$	0.011 M ≤ $[NO_2^-]$ ≤ 5.5 M	0.011 M ≤ $[NO_2^-]$ ≤ 5.5 M	0.011 M ≤ $[NO_2^-]$ ≤ 5.5 M
	$[NO_3^-]$/ ($[OH^-]$ + $[NO_2^-]$)	< 2.5	< 2.5	< 2.5
1.0M<$[NO_3^-]$ ≤ 3.0 M	$[OH^-]$	0.1 ($[NO_3^-]$) ≤ $[OH^-]$ < 10 M	0.1 ($[NO_3^-]$) ≤ $[OH^-]$ < 10 M	0.1 ($[NO_3^-]$) ≤ $[OH^-]$ < 4.0 M
	$[OH^-]$ + $[NO_2^-]$	≥ 0.4 ($[NO_3^-]$)	≥ 0.4 ($[NO_3^-]$)	≥ 0.4 ($[NO_3^-]$)
$[NO_3^-]$ > 3.0 M	$[OH^-]$	0.3 M ≤ $[OH^-]$ < 10 M	0.3 M ≤ $[OH^-]$ < 10 M	0.3 M ≤ $[OH^-]$ < 4.0 M
	$[OH^-]$ + $[NO_2^-]$	≥ 1.2 M	≥ 1.2 M	≥ 1.2 M
	$[NO_3^-]$	≤ 5.5 M	≤ 5.5 M	≤ 5.5 M

As retrieval of waste and return streams to the tanks start to occur, once the radioactive waste stabilization operations are online, the chemistry of the tank supernates may change significantly. The chemistry may shift to lower pHs and be more concentrated with aggressive species (e.g., chloride, sulfate, etc.) than is observed in the current waste chemistry. Therefore, the corrosion control program is being evaluated to adapt to anticipated changes in chemistry.

Testing for pitting corrosion has been performed using the standardized Cyclic Potentiodynamic Polarization (CPP) test developed by TIEP-CSG [3] and presented in
Table 2-2.

Table 2-2 Standardized CPP protocol with the parameters utilized for testing

Parameters	Results
Potential Stabilization (hrs.)	2
Start Potential (V vs. OCP)	-0.05
Scan Rate (mV/s)	0.167
Vertex Threshold (mA/cm^2)	1
Finish Potential (V vs. OCP)	0
Sample geometry	bullet
Surface Preparation	600 grit

SRNL has used the standardized CPP protocol to develop comprehensive new limits to prevent pitting corrosion and establish guidelines for a more robust chemistry control. The testing initiated in FY16 used a test matrix from Plackett-Burman and Box-Behnken statistical designs. From the experiments, the significant aggressive species identified were nitrate and chloride, while significant inhibitor species were hydroxide and nitrite at specific ranges of chemistries based on tank chemistry [4]. In FY17, electrochemical experiments were expanded to include high hydroxide concentrations and additional interior points. The results combined consisted of 95 individual tests with duplicates. A logistic regression analysis resulted in Equation 1.

$$\text{Lin}(0) = 0.60 + 8.40\,[OH^-] + 2.37\,[NO_2^-] - 0.98\,[NO_3^-] - 19.32\,[Cl^-] \qquad \textbf{Equation 1}$$

A pitting factor was obtained and utilized as a basis for corrosion control requirements for waste chemistry. A previous report [5] established the rationale for using a pitting factor as a practical criterion for corrosion control. Assuming the value of the coefficient was representative of the relative contribution to either pitting or inhibition, then the ratio of inhibitor to aggressive species could be utilized as a criterion for failure. The pitting factor was designated as shown in Equation 2,

$$\text{Pitting Factor} = \frac{\text{Inhibitor Species}}{\text{Aggressive Species}} = \frac{8.52\,[OH^-]+2.41\,[NO_2^-]}{[NO_3^-]+19.6\,[\text{Halide}]} \qquad \textbf{Equation 2}$$

where halide concentration is the sum of the chloride and the fluoride concentrations. The use of halide, instead of chloride, was used since fluoride concentration did not initially appear to be a significant variable within the ranges of all tested variables. A primary reason is the low solubility of fluoride in the more concentrated solutions. However, in more dilute solutions, at low chloride levels, the fluoride is present and is a known pitting agent for carbon steel [6]. This reference further states that the pitting potentials are more positive and corrosion rates are lower in the presence of fluorides than those found for similar chloride concentrations. Thus, it is a conservative assumption to assign the same coefficient in the pitting factor relationship as the chloride anion.

The pitting factor developed during New Limits testing showed that pitting factors less than 1 are indicative of pitting susceptibility with a high degree of confidence. Pitting factors between 1 and 2 are unlikely to result in pitting but may pit at high aggressive species concentrations even in well inhibited solutions. Pitting factors greater than 2 are indicative of a condition that is not expected to cause pitting. From the results of 95 tests**,** ~ 94% of these were accurately predicted by the pitting factor, demonstrating the efficacy to use this criterion for the determination of pitting corrosion based on significant species in the waste chemistry.

2.2 Secondary Liner Corrosion Inhibition

There are 28 DSTs at Hanford Site. Each DST consists of a primary shell (inner) surrounded by secondary (outer) shell. The secondary shell rests on a concrete pad. A schematic diagram for some double shell configurations (e.g., AY, AZ and SY Tank Farms), shows the concrete foundation and drain slots and is presented in Figure 2-1.

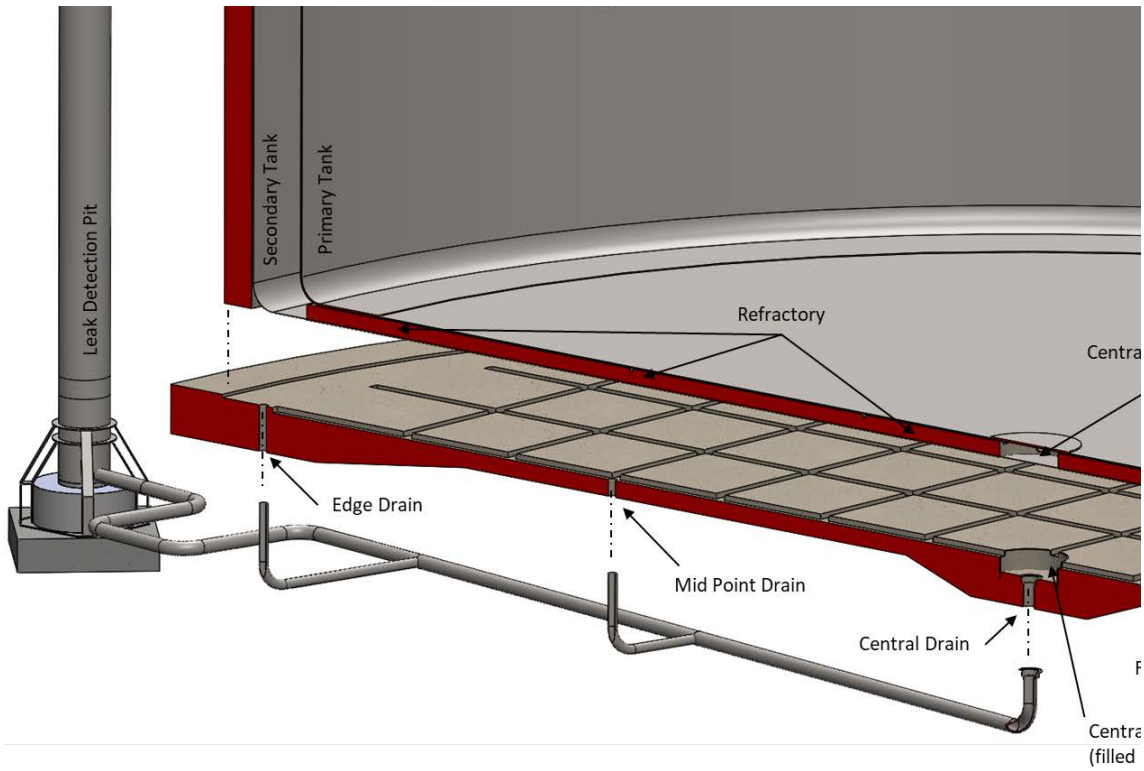

Figure 2-1 Schematic of a double shell tank depicting primary and secondary tank shells, concrete foundation, and drain slots.

Water is known to accumulate in the drain slots and cause corrosion on the exterior of the secondary liner. Ultrasonic inspection is confined to the annular space between the primary and secondary tanks, leaving a concern that corrosion is widespread on the underside of the bottom plate. Since the water level can vary in the drain slots based on accumulation, corrosion could be caused by direct contact with the accumulated water or when the water level is below the underside of the tank bottom, VSC could also occur. Accumulated water is drained through the sumps into leak detection pits. The drained water was analyzed for its constituents, and two simulants were developed considering the chemical composition range of the accumulated water. The simulants were identified as LDP and GW.

Testing with LDP and GW simulants for legacy carbon steel corrosion was started in FY14 with a long term immersion experiment in which the deleterious effects of these chemistries were observed, with mass loss corrosion rates obtained of approximately 10 mpy [7][8]. During FY16 testing was focused on the inhibition strategies using commercial VCI to coat the samples and minimize VSC and other types of corrosion. Testing continued during FY17 and it was observed that by coating the samples with VCI, the corrosion inhibition was short-lived and did not significantly reduced carbon steel corrosion [5]. For this section, the objective is to find other VCI strategies that can effectively minimize corrosion of carbon steel exposed to LDP and GW.

2.3 Anodic drift studies

Approximately 55 million gallons of radioactive waste is being stored in 177 carbon steel tanks at Hanford. Long-term performance and integrity of the tanks is partly dependent on modifying the

waste chemistry such that risk of pitting and stress corrosion cracking of the tank carbon steel are mitigated. To this end, CPP experiments are conducted to identify risk of pitting corrosion, and subsequently determine the level of inhibition needed to mitigate pitting corrosion. One of the key parameters associated with the determination is the difference between the corrosion and repassivation potentials: if the corrosion potential is greater than repassivation potential, the risk of pitting corrosion exists. Corrosion potential is defined as steady-state value of OCP.

CPP experimental data is generally used to measure tendency of repassivation including repassivation potential, and it is assumed that corrosion potential is held steady during the measurement and thereafter. It is implicitly assumed that the corrosion potential measured at the start of CPP is sufficient for risk analysis. However, it has been observed that certain simulated waste chemistries lead to significant change in OCP over time, and a steady-state value of OCP becomes the corrosion potential. A distinction is drawn between OCP and corrosion potential. At the corrosion potential, rates of anodic and cathodic reactions balance each other, and the metal surface is in equilibrium with the surrounding electrolyte. OCP is defined when the metal surface is in the process of establishing equilibrium with the surrounding electrolyte, and there is an imbalance between the rate of anodic and cathodic reactions. When the rate of anodic and cathodic reactions are balanced, OCP becomes the corrosion potential of a metal surface in a given electrolyte. The change in OCP during CPP tests could lead to underassessment of the risk, especially when corrosion potential is below the repassivation potential, and difference between the two is sufficiently low such that an upward drift in OCP would increase the risk of corrosion potential exceeding the repassivation potential, and thereby, increasing the risk of localized corrosion in form of pitting corrosion.

Another key difference between laboratory testing using CPP and field conditions has been the surface condition of coupons used in the laboratory testing in comparison with the field condition of the tanks. CPP tests have been conducted using the bullet coupons with 600 grit ground surfaces [4],[5],[7],[8] whereas the tanks were constructed using the steel with mill scale plus corrosion products. It is recognized that during the construction process, large sheets of the carbon-steel metal were welded together, and other processes associated with tank construction likely have disturbed the original mill-scale on portions of the tank liner. Considering this, a 600 grit ground coupon was utilized as one extreme of the surface condition whereas a coupon with mill-scale plus corrosion products is considered the other extreme. The surface condition of a newly constructed tank is expected to be somewhere between the two extremes. In addition, the tanks were put in service sometime after completion of construction. This would have provided the tank steel to get exposed to ambient conditions and develop additional layers or corrosion products before being placed in service. Considering several possibilities of the surface conditions, the objective of the study also included determining effect of surface condition on evolution of OCP. The objective also included establishing conservatism of the CPP tests results, i.e., the tests results sufficiently bound the conclusions derived from the test data.

2.4 Quartz-Enhanced Photoacoustic Spectroscopy (QEPAS) studies

QEPAS is a pass-through type method for measuring trace impurities in gas streams. In the simplest sense, QEPAS works by using a quartz-tuning fork (QTF) to detect sound generated by the local heating of gas through the relaxation of excited molecules. Sound generated at specific frequencies causes oscillations to occur in the QTF, resulting in charge generation proportional to the concentration of the absorbing gas. Importantly, each gas target has a unique frequency mode(s) that can be vibrationally excited by the laser; therefore, tuning the laser to specific modes allows

for the detection of specific gases. Using QEPAS, SRNL can monitor real time (1 to 10 second intervals) gas concentration changes within the parts per million range.

During FY16 and FY17, modest efforts to investigate the use of QEPAS as an ammonia sensor were initiated by SRNL [9]. It has been demonstrated that the presence of ammonia in the vapor phase can inhibit vapor space corrosion of carbon steel [10],[11]. Throughout FY17, significant progress was made towards proving operational feasibility of a QEPAS sensor within conditions such as those found at Hanford.

3.0 Task Description and Activities

Several tasks were performed during FY18 and are described in the sections below.

3.1 Task 1: New Limits Testing

The New Limits Testing for FY18 consisted of two parts; immersion testing and electrochemical testing. The results for this task are organized in section 5.1 and 5.2

3.1.1 *Immersion Testing*

Statistical design methods were used to create a matrix for twenty-five concentrations of statistically significant variables (i.e., hydroxide, nitrite, nitrate, chloride) to provide a long-term corrosion assessment of partially and completely immersed coupons. The test duration was four months in which pH and OCP measurements were recorded periodically.

3.1.2 *Electrochemical Testing*

Testing using electrochemical methods was performed in FY18 to study borderline conditions in pitting factor calculations (i.e., pitting factors between 1 and 2). Fifteen tests were selected at a set of concentrations for hydroxide and nitrite with changing nitrate and chloride concentrations. Tank chemistry simulants were also tested corresponding to tanks AN-107, AN-102, AP-104, AP-106, AW-101 and AW-103. Most of these tanks presented a pitting factor 1 to 2, except AW-101. Tank simulant chemistries corresponding to AP-104 and AW-103, with and without fluoride, were utilized while maintaining the total concentration of halides (i.e., chloride and fluoride) to study fluoride effects. An additional nine tests were statistically designed to expand the study of fluoride effects for a more critical analysis into halide effects in the pitting factor.

3.2 Task 2: Secondary Liner Corrosion Testing

Several experiments were setup with GW simulant as the base electrolyte with legacy carbon steel disk coupons. Vapor corrosion inhibitors experiments included (a) as-prepared GW simulant plus Calcium Carbonate ($CaCO_3$), (b) coupons exposed to a mixture of GW simulant plus VCI-A, and (c) coupons exposed to a mixture of GW simulant plus VCI-B. The two VCI strategies will be discussed in the experimental section for this task. The VSC setup was used to test the different strategies to determine its efficacy to prevent corrosion while coupons were immersed and at a vapor phase at three different levels. The tests with $CaCO_3$ were performed to assess a potentially representative condition without the VCIs present. The $CaCO_3$ may be leached from the concrete

and alter the pH (i.e., more basic) sufficiently that the VCI is not necessary. The results for this part are presented in section 5.2.

3.3 Task 3: Anodic Drift Studies

A total of three corrosion cells were setup, each with a working electrode that had a different surface preparation. The first electrode was a 600-grit ground bullet coupon, routinely used in the CPP tests. The second electrode was a cut out from a rail-road car steel piece with mill-scale and corrosion product on one face of the coupon. The third electrode was prepared in the same manner as the second electrode except that part of the coupon surface was scuffed with 300 grit sand paper. This action was implemented to partially remove corrosion products and mill-scale on the coupon surface. Scuffing of the surface was to emulate potential changes to the surface during construction. OCP measurements were taken for a period of four months, and at the end the standard CPP protocol was used to determine pitting susceptibility. The results obtained for this task are shown in section 5.3.

3.4 Task 4: QEPAS studies

The QEPAS studies at SRNL during FY18 can be broken into four parts; sensor procurement, calibration, humidity studies, and vapor space corrosion (VSC) cell monitoring. A new Acoustic Detection Module (ADM) was purchased from Achray Photonics Inc. The ADM shown in Figure 3-2 is the functioning portion of the QEPAS system. In the field, the ADM can be separated from the laser, control electronics unit (CEU), and gas control if desired. The ADM is relatively small with a volume of ~1 cubic inch. As such, building a portable system would require the laser, CEU, and gas control systems to be optimized; however, the size of the ADM would not need to be changed. These components can be easily modified to fit within a small suitcase sized container, allowing for a completely portable system. Shown in Figure 3-2 is an example of a compact system designed by Viola et. al [12] that was able to maintain low limits of detection in the range of ppb. Details on the humidity, calibration, and vapor cell tests will be presented in Section 5.4

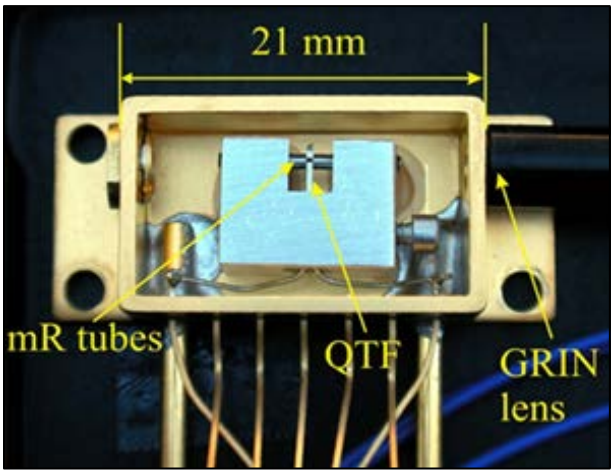

Figure 3-1 QEPAS Acoustic Detection Module (ADM)

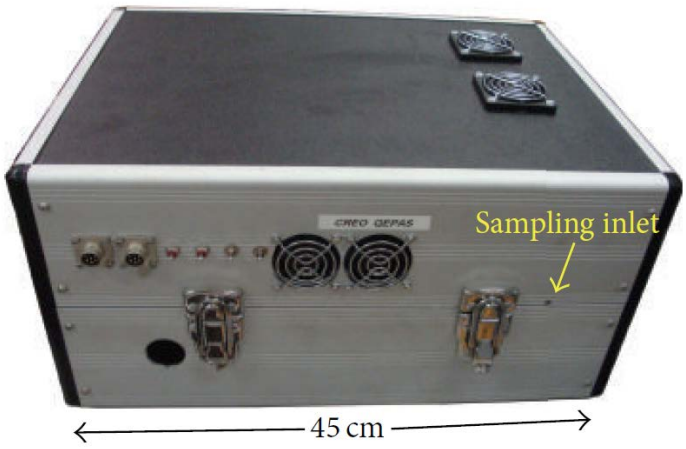

Figure 3-2 Modular QEPAS sensor package developed by Viola et. al that measures approximately 17 in x 13 in x 9 in. [10]

4.0 Experimental Procedure

The material used for all corrosion testing is carbon steel selected from AAR TC128 Rail Car Steel. This steel was selected for testing since it approximates the chemistry and microstructure of American Society for Testing and Materials (ASTM) A515, Grade 60 carbon steel, the steel from which the tanks were fabricated [13]. The chemical composition of the steel is shown in Table 4-1

Table 4-1 Chemical Composition of AAR TC128 Rail Car Steel

	C	Mn	P	S	Si	Fe
Specification (wt%)	0.24 (max.)	0.9 (max.)	0.035 (max.)	0.04 (max.)	0.13 to 0.33	Balance
Measured (wt%)	0.212	1.029	0.012	0.013	0.061	Balance

In the next pages are the experimental details and conditions in which the carbon steel was used and prepared for electrochemical testing, secondary liner corrosion testing, and complete and partial long immersion testing.

4.1 Long-term testing using complete and partial immersed coupons

4.1.1 *Material sample*

Coupons 2 inch long, 1 inch wide and 0.063 inch thick (Metal Samples part number CO101) with a 0.1875 inch hole at the top were used for long-term immersion testing. The coupons were requested to be ground to a 600 grit finish. To measure electrochemical response on 25 of the coupons, used for complete immersion, a wire was attached to the sample by threading it into the hole and mounting it with epoxy (EpoKwick from Buehler). Figure 4-1 shows a picture of a coupon mounted in epoxy connected with a purple coated wire.

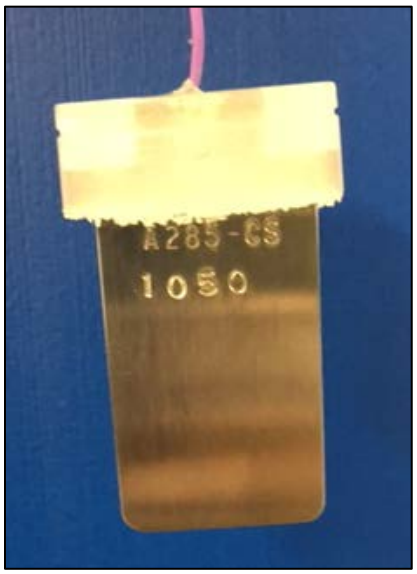

Figure 4-1 Rectangular coupon used in immersion testing mounted in epoxy and electrically connected using a purple coated wire (engraving error for the carbon steel as A285).

4.1.2 *Simulants*

Simulants prepared for the new limits testing for long-term experiments are shown in Table 4-3. The statistical software JMP® v. 11.1.1 from SAS Institute Inc. was used to prepare the test matrix. Twenty-five chemistries were chosen at hydroxide concentrations of 0.0001, 0.1, 0.3 and 0.6 M and nitrite concentrations of 0, 0.6 and 1.2 M. Nitrate and chloride concentrations were then statistically selected to account for different chemistries.

Table 4-2 Immersion test statistically selected simulant chemistries

Test	Hydroxide (M)	Nitrite (M)	Nitrate (M)	Chloride (M)	Sulfate (M)	TIC (M)	Pitting Factor*
1	0.0001	0	0.153	0.049	0.2	0.1	0.00
2	0.0001	0	0.234	0.040	0.2	0.1	0.00
3	0.0001	0.6	0.154	0.050	0.2	0.1	1.28
4	0.0001	0.6	0.585	0.017	0.2	0.1	1.58
5	0.0001	1.2	0.023	0.058	0.2	0.1	2.49
6	0.0001	1.2	0.797	0.005	0.2	0.1	3.23
7	0.1	0	0.081	0.094	0.2	0.1	0.44
8	0.1	0	0.984	0.047	0.2	0.1	0.45
9	0.1	0.6	0.452	0.073	0.2	0.1	1.22
10	0.1	0.6	1.686	0.007	0.2	0.1	1.26
11	0.1	1.2	0.076	0.094	0.2	0.1	1.95
12	0.3	0	0.325	0.155	0.2	0.1	0.76
13	0.3	0	0.715	0.135	0.2	0.1	0.76
14	0.3	0	1.721	0.072	0.2	0.1	0.82
15	0.3	0	2.616	0.017	0.2	0.1	0.87
16	0.3	0.6	2.764	0.006	0.2	0.1	1.39
17	0.3	1.2	1.132	0.111	0.2	0.1	1.65
18	0.3	1.2	2.201	0.042	0.2	0.1	1.80
19	0.6	0	0.216	0.293	0.2	0.1	0.86
20	0.6	0	1.021	0.233	0.2	0.1	0.91
21	0.6	0	2.444	0.144	0.2	0.1	0.97
22	0.6	0	4.303	0.013	0.2	0.1	1.12
23	0.6	0.6	1.020	0.234	0.2	0.1	1.17
24	0.6	0.6	2.985	0.099	0.2	0.1	1.33
25	0.6	1.2	4.224	0.018	0.2	0.1	1.75

*Equation 2 used to calculate pitting factor.

4.1.3 *Testing Apparatus*

1 L capacity polypropylene (PP) bottles were used. The caps of the bottles were modified. Stoppers were added to the caps and used to connect flexible tubing to provide an inlet and outlet flow of humidified air and to maintain the glass holders that held the coupons in position. A hole in the middle was used to provide access for a pH probe, a thermocouple, and a reference electrode. The hole was closed off with a rubber stopper when not in use.

Two coupons were used for each bottle. One coupon was connected to a purple coated wire that was previously mounted with epoxy. OCP measurements were taken from this completely immersed coupon. The other coupon was partially immersed to investigate the corrosion behavior at the LAI and VS. The coupons were rinsed with distilled water and acetone prior to immersion.

Figure 4-2 (a) shows a picture of the coupons mounted on a glass holder for partial and complete immersion. This configuration was placed in the PP bottle as shown in Figure 4-2 (b). In each of the PP bottles, 600 mL of the simulant was added. The PP bottles were placed in a water bath inside a stainless-steel container. The container was placed on top of a hotplate for temperature control. Temperature was maintained at 35 °C. Air was supplied at a flow rate of 10 sccm to a bubbler that humidified the air and circulated it through the PP bottles. Figure 4-3 displays all the PP bottles that were placed in the water bath in two containers. Container #1 (right) contained sixteen PP bottles and container #2 contained nine PP bottles. Styrofoam pellets, which floated on the water, were used to minimize water evaporation. Steady state conditions were maintained for four months. Water was added periodically to the bath to maintain the same level. Make-up distilled water was added occasionally to the PP bottles to maintain the LAI level. pH, temperature and OCP were measured almost daily during working days. The coupons were maintained at this temperature for four months. At the end of testing the coupons were removed and cleaned using ASTM G1 C.3.1 solution to obtain weight losses and to inspect visually for areas of corrosion [14]. 3-D Measuring Macroscope images using a Keyence VR-3000 were performed for all coupons to assess the corrosion attack sustained.

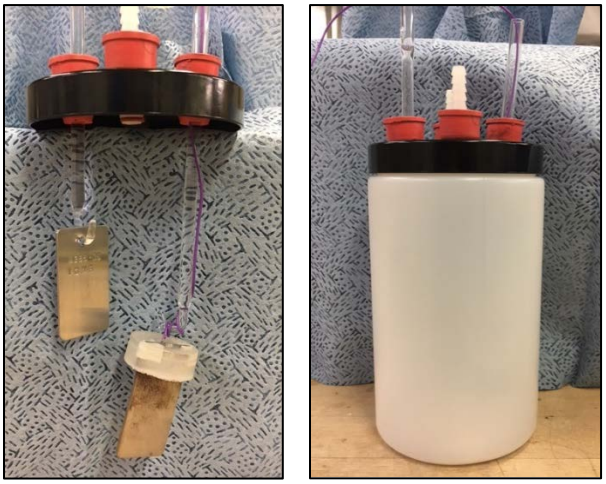

(a) **(b)**

Figure 4-2 Immersion test setup showing (a) the configuration of the coupons for LAI and immersion and (b) the coupons inside the PP bottle

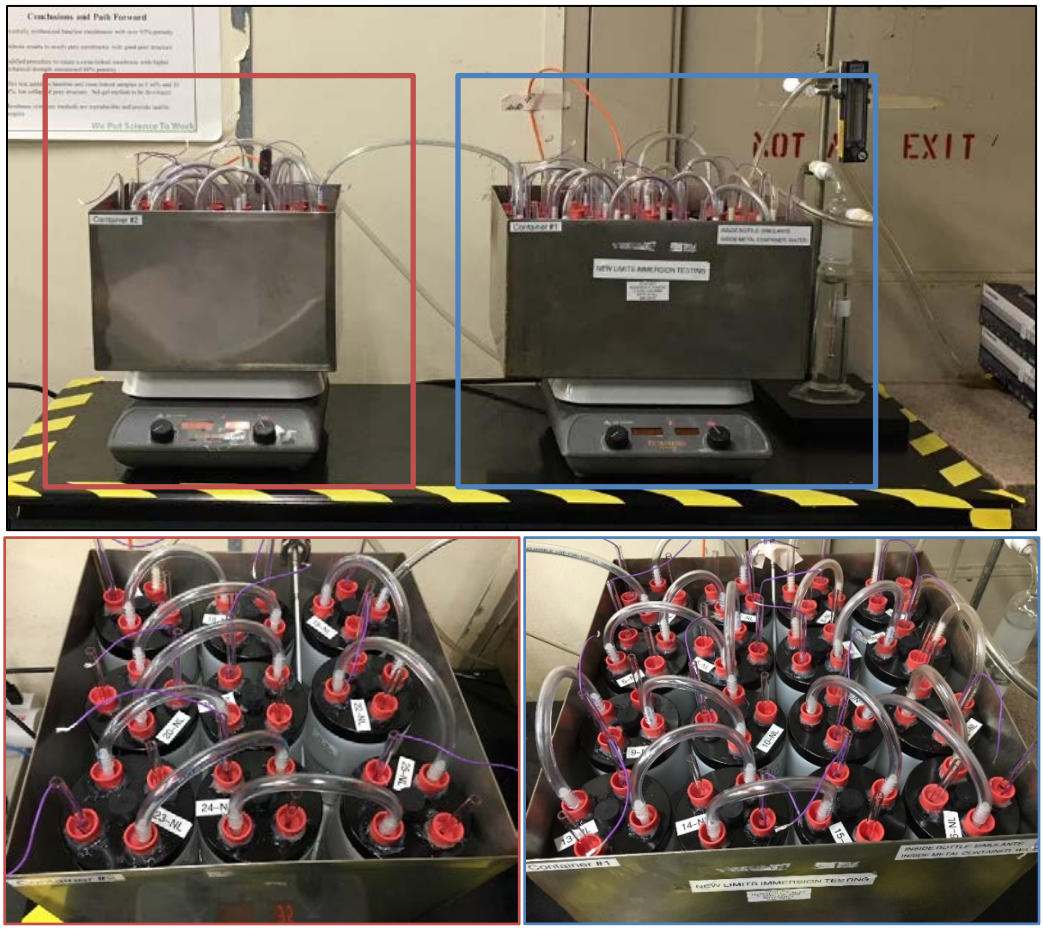

Figure 4-3 Immersion test setup showing the two stainless steel water baths next to each other and top pictures of the inside of each container.

4.2 Electrochemical Testing of Simulants

4.2.1 *Material sample*

The electrochemical testing was performed by using electrodes in "bullet" shape with dimensions: 0.188 inch in diameter and 1.25 inches long (Metal Samples Company part number EL-400). In Figure 4-4, it shows a picture of the sample after being ground and rinsed. Before testing, a drill was used to rotate the sample and grind it to a uniform 600 grit finish. After, the sample was rinsed with distilled water and acetone. The bullets were examined visually for any defect and to ensure that the sample had a uniform surface preparation. The sample was then attached to a stainless-steel rod protected by a glass holder. A polytetrafluoroethylene (PTFE) fixture was used to prevent liquid contact with the stainless-steel rod and therefore to ensure electrical isolation.

Figure 4-4 Side picture of the "bullet" shape sample

For anodic drift testing, two additional samples were created by cutting 2 inches by 2 inches squares of AAR TC128 metal mill-scale side with no further surface preparation. The material was cut using an Electrical Discharge Machine (EDM). The samples were connected to a wire for electrical connection using silver epoxy, then mounted with a two-part clear epoxy solution (EpoKwick from Buehler) so that one face of the coupon was exposed. One of the two coupons was scuffed with 300 grit sand paper over part of the surface. Figure 4-5 show images of the two coupons used for this task. The coupon area for the second coupon which was scuffed with sand paper is highlighted by a red rectangle.

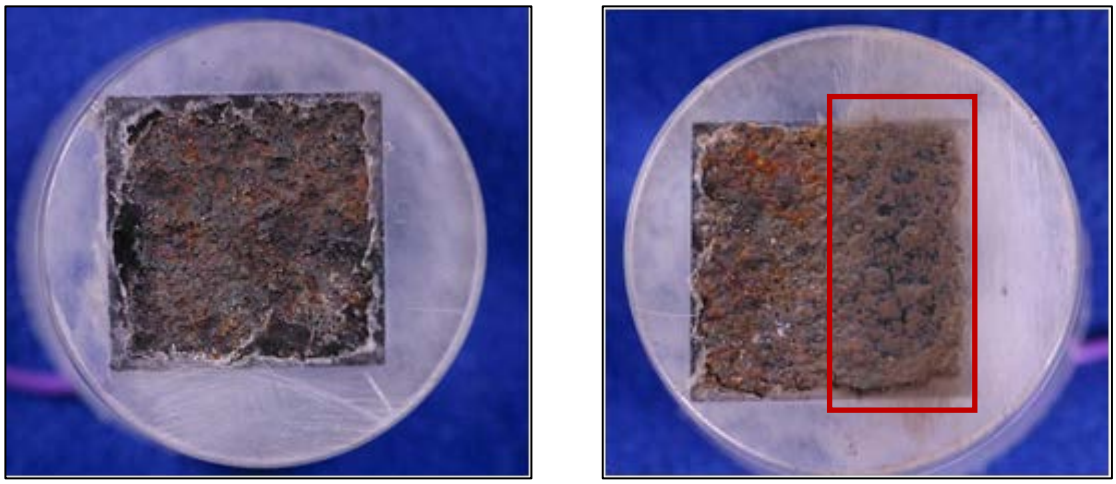

(a) Coupon cut out of rail road car steel with mill-scale plus corrosion product on the exposed surface

(b) Coupon cut out of rail road car steel with mill-scale plus corrosion product on the exposed surface. Part of the coupon surface, highlighted by red rectangle, was scuffed with 300 grit sand paper

Figure 4-5 Images of the coupons used to study evolution of OCP as a function of surface condition in AN-107 simulant

4.2.2 *Simulants*

For New Limits testing (Task 1), sixteen simulants were prepared to obtain chemistries with pitting factors between 1 and 2 that were selected based on changing the concentration of significant species with a range of high to low concentration of nitrate, nitrite, hydroxide and chloride. The simulants are listed in Table 4-3. In the instances, that the pitting factor was higher than 2, the values are presented highlighted in yellow. Additional waste tank simulants corresponding to more complex chemistries were selected with mostly pitting factors between 1 and 2 and close to 2, with one notable exception, test 23. These are highlighted in orange. These corresponds to AN-102 (16), AN-107 (17), AP-104 (19), AP-106 (20), AW-103 (22) and AW-101(23). Two tank simulants tests corresponding to AN-107 (18) and AW-103 (21) maintained the total halide chemistry of the original simulant but the fluoride concentration was substituted with additional chloride.

Table 4-3 Simple chemistries and tank chemistries simulants at pitting factors generally between 1 and 2.

Test	Hydroxide (M)	Nitrite (M)	Nitrate (M)	Chloride (M)	Fluoride (M)	Sulfate (M)	TIC (M)	Pitting Factor*
1	0.0001	0.6	0.3	0.04	0	0.2	0.1	1.33
2	0.0001	1.2	0	0.05	0	0.2	0.1	2.95
3	0.0001	1.2	2	0	0	0.2	0.1	1.45
4	0.1	0	0.2	0.02	0	0.2	0.1	1.44
5	0.1	0.6	0.3	0.06	0	0.2	0.1	1.56
6	0.1	1.2	0.5	0.05	0	0.2	0.1	2.53
7	0.1	1.2	2.5	0.005	0	0.2	0.1	1.44
8	0.3	0	0.1	0.08	0	0.2	0.1	1.53
9	0.3	0.6	0.07	0.1	0	0.2	0.1	1.97
10	0.3	1.2	0.5	0.15	0	0.2	0.1	1.58
11	0.3	1.2	2.5	0.05	0	0.2	0.1	1.57
12	0.6	0	0.6	0.05	0	0.2	0.1	3.24
13	0.6	0.6	0.001	0.25	0	0.2	0.1	1.34
14	0.6	1.2	0.001	0.3	0	0.2	0.1	1.36
15	0.6	1.2	5.5	0.01	0	0.2	0.1	1.41
16	0.611	1.99	3.13	0.101	0.001	0.2	0.1	1.95
17	0.42	1.4	2.99	0.05	0.01	0.2	0.1	1.67
18	1.03	1.37	2.44	0.14	0	0.2	0.1	2.33
19	1.03	1.37	2.44	0.08	0.06	0.2	0.1	2.33
20	0.37	1.02	1.25	0.1	0	0.2	0.1	1.75
21	0.884	0.771	1.578	0.291	0	0.2	0.1	1.29
22	0.884	0.771	1.578	0.073	0.218	0.2	0.1	1.29
23	5.76	2.33	2.79	0.19	0.04	0.2	0.1	7.49

*Equation 2 used to calculate pitting factor.

Additional experiments were performed with simple simulants to determine fluoride effects in the pitting factor coefficient. The simulant constituents were statistically selected and are listed in Table 4-4. For this case, no duplicate electrochemical experiments were run since the tests already contained a duplicate in the matrix in most cases.

Table 4-4 Simulant chemistries to determine fluoride effects

Test	Hydroxide (M)	Nitrite (M)	Nitrate (M)	Chloride (M)	Fluoride (M)	Sulfate (M)	TIC (M)	Pitting Factor*
1	4	2	0	0.4	0.3	0.2	0.1	2.84
2	4	2	0	0.4	0.3	0.2	0.1	2.84
3	0.0001	2	4	0.4	0.3	0.2	0.1	0.27
4	0.0001	2	4	0.4	0.3	0.2	0.1	0.27
5	4	0	4	0.4	0	0.2	0.1	2.88
6	4	0	4	0.4	0	0.2	0.1	2.88
7	4	2	0	0	0.3	0.2	0.1	6.62
8	4	2	0	0	0.3	0.2	0.1	6.62
9	4	0	4	0	0.3	0.2	0.1	3.45
10	4	2	0	0	0	0.2	0.1	N/A
11	4	0	4	0.4	0	0.2	0.1	2.88
12	4	2	4	0	0	0.2	0.1	9.73
13	0.0001	2	4	0.4	0.3	0.2	0.1	0.27
14	0.0001	2	4	0.4	0.3	0.2	0.1	0.27
15	4	0	0	0.4	0.3	0.2	0.1	2.48

*Equation 2 used to calculate pitting factor.

For anodic drift, the simulant selected was Test 17 from Table 4-3 corresponding to AN-107 simulant. The complete composition of this simulant is given in Table 4-5.

Table 4-5 Chemical composition of the AN-107 simulant used to study evolution of OCP

Simulant source	Concentration (M)	Simulant source	Concentration (M)
Aluminum nitrate, 9-hydrate	0.1000	Disodium EDTA ($Na_2C_{10}H_{14}O_8.2H_2O$)	0.0540
Ferric nitrate, 9-hydrate	0.0310	HEDTA ($C_{10}H_{18}N_2O_7$)	0.0213
Calcium nitrate, 4-hydrate	0.0142	Nitrilotriacetic Acid	0.0085
Lead nitrate	0.0017	Iminodiacetic Acid	0.1265
Nickel nitrate, 6-hydrate	0.0094	Sodium gluconate	0.0284
Manganese dichloride	0.0139	Sodium hydroxide	2.1251
Potassium nitrate	0.0457	Sodium formate	0.4450
Sodium chloride	0.0222	Sodium acetate, 3-hydrate	0.0397
Sodium fluoride	0.0100	Sodium oxalate	0.0134
Sodium sulfate	0.0700	Sodium carbonate	1.4300
Sodium phosphate, 12-hydrate	0.0300	Sodium nitrate	2.5007
Glycolic acid	0.3080	Sodium nitrite	1.4000
Citric acid, 1-hydrate	0.1250		

4.2.3 *Testing Apparatus*

Approximately 700 mL of simulant was added into a glass cell made by the SRNL glass shop similar to the corrosion cell designed by Princeton Applied Research (AMETEK). A carbon graphite rod served as the counter electrode. A saturated calomel electrode (SCE) was used as the reference electrode and placed directly in the simulant for tests shorter than 9 hours and placed in a bridge with a glass frit for tests longer than 9 hours (e.g., anodic drift testing). Prior to each test, the electrode was checked against a standard (a SCE in 1 M KCl solution that was not used for testing) and several times during long term testing. The cell was placed on top of a hotplate with temperature control and the temperature was maintained by a thermocouple from the hotplate immersed in solution. REF600 and Interface E (Gamry) potentiostats were used in this study. Prior to initiating the electrochemical tests, ASTM G5 [15] was performed for quality assurance. ASTM G5 protocols were also run at the conclusion of testing. The standardized CPP protocol was used to gather the data.

For anodic drift testing, a multiplexer (Gamry) was used to obtain OCP data. Three cells were used with the same solution but a different surface on the sample. The first cell had a “bullet” sample

with 600 grit finished surface, the second cell had a mill-scale finish, and the third cell has a partial mill-scale finish. OCP was measure every 10 seconds for approximately 4 months. In several instances, Electrochemical Impedance Spectroscopy (EIS) scans were performed at several ranges of frequency. At the end of testing, the standard CPP protocol was used to test the susceptibility to localized corrosion. Figure 4-6 displays three pictures of the electrochemical setups used in anodic drift for the three coupons: bullet, mill-scale, partial mill-scale.

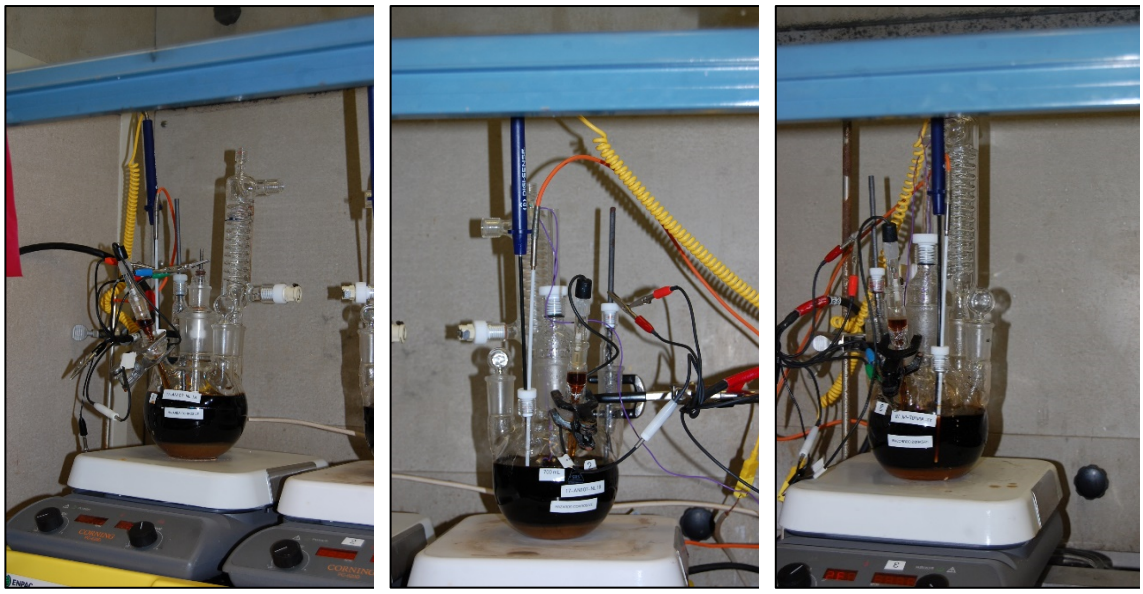

Figure 4-6 Images of the experimental setup used in the anodic drift studies. The three images are for the three separate setups used for the three coupons.

4.3 Secondary Liner Corrosion Testing

4.3.1 *Materials*

Circular coupons were sectioned from the railcar carbon steel stock of material. The coupons were 0.625 inch diameter with a thickness of 0.125 inch and were ground to a 600 grit finish at each side. The coupons were then engraved to identify them with a number from 1 to 24. A coated wire was placed in a lateral position to be able to hang the coupons with no electrical connection to the coupon. The coupons were mounted with a two-part clear epoxy solution (EpoKwick from Buehler) so that one face of the coupon was exposed. Prior to using the coupons, they were rinsed with distilled water, then acetone. The coupons are shown in Figure 4-7.

Figure 4-7 One coupon mounted in epoxy cold mount with wire

4.3.2 *Simulants*

GW simulant was used for the secondary liner corrosion studies. Composition of the GW simulant is provided in Table 4-6. The pH of the simulant was adjusted using sodium carbonate and acetic acid to 7.6 after preparation. Several VCI strategies were used. They included (1) as-prepared GW simulant plus $CaCO_3$, (2) coupons exposed to GW simulant plus VCI-A, and (3) coupons exposed to GW simulant plus VCI-B. VCI-A is VpCI-337, and it was mixed GW simulant in 10% V/V concentration, i.e., 100 mL in VpCI-337 plus 900 mL of simulant for 1 L of the VCI solution. VCI-B was a mixture of VpCI-645 + VpCI-609 and was mixed as 10% VpCI-609 by weight of solution (100 g VpCI-609 in 1 liter of GW) and 0.75% VpCI-645 by volume (7.5 mL/L of solution). VpCI-337, VpCI-645 and VpCI-609 are several product names for VCI formulations made commercially by Cortec®.

Table 4-6 Composition of Ground Water Simulants

Chemical	Concentration (M)
Sodium bicarbonate	1.750E-03
Calcium hydroxide	1.500E-03
Potassium nitrate	2.400E-04
Strontium Nitrate	2.874E-06
Ferric sulfate	6.250E-04
Sodium Metasilicate, 5hydrate	6.000E-04
Ferric chloride	7.667E-05
Manganese Chloride	3.100E-04
Acetic Acid	3.000E-04
pH adjusted using sodium carbonate and acetic acid	7.6

4.3.3 *Testing Apparatus*

A glass vessel of dimensions 3.3 ft tall and 5.5 inch diameter was used for each experiment. Approximately 1 L of either treated or untreated simulant was added to a vessel for each

experiment; treated simulant refers to a mixture of prepared simulant plus VCI, and untreated simulant refers to as-prepared simulant. Each vessel has a water jacket around the simulant holding area which was used to circulate warm water to maintain the simulant temperature at 45 ± 2 °C. Each vessel also has several ports, which were used to insert thermocouples and electrical resistance (ER) probes. An image showing the two vessels used is presented in Figure 4-8(a). Coupons were exposed to the electrolyte and vapors of the electrolyte in each experiment by suspending them through a rod shown in Figure 4-8(b). The rods holding the coupons were placed inside the vessels. Coupons were suspended from stainless steel rings that are welded to a stainless-steel rod at three different locations. Three vessels were used and for these vessels two coupons were placed at the top, intermediate and low position. Also, two coupons were placed lower than the low position, so they can be immersed into the solution. The coupons' positions, with respect to electrolyte in each vessel, simulated different vapor space conditions and water levels in the drain slots. These levels are described as follows.

Level 1: Bottom or low level. Coupons were dipped in the simulant for five minutes prior to testing. The coupons were hung at the bottom fixed ring of the rod shown in Figure 4-8(b). These coupons were suspended approximately 1 inch above the liquid level of the simulant. Every two weeks, the coupons were lowered into the simulant for 5 minutes. This level is representative of the situation when secondary liner bottom plate experienced periodic wetting/drying.

Level 2: Intermediate or middle level. Coupons were dipped in the simulant for five minutes prior to testing. The coupons were hung at the middle-fixed ring approximately 18 inches above the liquid simulant in each vessel. This level is representative of a vapor space region of the secondary liner bottom that at one time was exposed to water but has infrequent or no contact with the water. However, this region is exposed to the humidified air.

Level 3: Top or high level. This set of coupons was not exposed to the solution prior to testing. The coupons were suspended approximately 36 inches above the simulant. This level is representative of the secondary liner bottom plate region that is only exposed to the humidified air and any volatile species from the solution.

(a) (b)

Figure 4-8 Images of the (a) experimental configuration, and (b) steel rod to suspend the coupons inside the vessel containing electrolyte.

ER probes were placed in each vessel, for the second and third VCI strategy, near the coupons at Level 1. ER probe data was collected periodically. Coupons were removed after several months of exposure and cleaned with Clarke's solution [14] to remove corrosion products and report accurate weight losses.

5.0 Results and Discussion

Solutions for New Limits Immersion Tests are listed in Appendix A. The pictures of the coupons after exposure and after cleaning of New Limits chemistries are shown in Appendix B. Selected coupons based on corrosion chemistry were analyzed using a 3-D measuring macroscope and height-colored images are displayed in Appendix C. CPP and pictures of the samples for the New Limits testing of chemistries with pitting factors between 1 and 2 and for fluoride effects are shown in Appendices E and F, respectively. Also included in these two appendices, are any modified ASTM G192 testing that was performed due to inconclusive results from CPP. Secondary liner GW solution and pictures of the samples after exposure and cleaning are shown in Appendix G and H, respectively. The results and discussions for the report are enumerated by the corresponding task.

5.1 New Limits

5.1.1 Immersion tests

Immersion tests were performed to study corrosion mechanisms that can occur during long term exposure to chemistries with significant species in a wide range of concentrations corresponding to various pitting factor values. The test was conducted for four months with two coupons per test set up: 1) a coupon partially immersed to assess LAI and VS corrosion and 2) a completely immersed coupon to assess general and pitting corrosion. The immersed coupon was mounted with a purple coated wire to provide OCP measurements for determining corrosion activity. After four months, the coupons were removed and cleaned to calculate mass loss and determine corrosion attack by analyzing the sample with a 3-D Measuring Macroscope.

The mass loss values after testing and cleaning are presented in Table 5-1 and Table 5-2 for tests in container #1 and container #2, respectively. The pitting factors are also shown in the tables. The visual evidence of the corrosive attack on each coupon is shown in Appendix B. The general corrosion rate was utilized to assess the performance of the totally immersed coupons. In general, these coupons correlated well with the corrosion rate by observation of the corrosion sustained (i.e., high general corrosion rates were indicative of large patches of corrosion, while low general corrosion rates correlated with small or limited patches of corrosion). The partial immersion coupons allowed for the assessment of LAI and VS corrosion. The following subjective criteria were utilized to assess these coupons.

Severe: Significant corrosion occurs both above and below the LAI (i.e., pits from 2-8 mils deep). Allowing the steel surface to be exposed to these conditions could lead to significant degradation.

Minor: Surface corrosion occurs at and above the LAI, with minimal or no corrosion below (<< 1 mpy). Allowing the liquid level to remain constant at this level for a significant period of time while exposed to these conditions increases the possibility of LAI corrosion.

No Attack: Surface corrosion occurs only in the VS and is clearly above the LAI. This attack may have initiated due to condensation or humid air. A stagnant liquid-air interface at this waste chemistry is relatively benign and produces only minor attack in the vapor space.

Table 5-1 Weight losses of coupons in container #1

Vessel number	Pitting Factor*	Coupon number	Level in vessel	mass loss (g)	Corrosion rate (mpy) or degree
1	0.00	1001	Partial	2.4015	Severe
		1002	Complete	0.3402	1.86
2	0.00	1003	Partial	1.4117	Severe
		1004	Complete	0.3721	2.04
3	1.28	1005	Partial	0.7999	Minor
		1006	Complete	0.0601	0.33
4	1.58	1007	Partial	0.2889	Minor
		1008	Complete	0.0750	0.41
5	2.49	1009	Partial	0.4572	Minor
		1010	Complete	0.0552	0.30
6	3.23	1011	Partial	0.2141	Minor
		1012	Complete	0.0413	0.23
7	0.44	1013	Partial	1.6992	Severe
		1014	Complete	0.1831	1.00
8	0.45	1015	Partial	0.0527	Minor
		1016	Complete	0.0330	0.18
9	1.22	1017	Partial	0.4122	Minor
		1018	Complete	0.0796	0.44
10	1.26	1019	Partial	0.1833	None
		1020	Complete	0.0595	0.33
11	1.95	1021	Partial	0.4030	None
		1022	Complete	0.0314	0.17
12	0.76	1023	Partial	0.7483	Minor
		1024	Complete	0.0671	0.37
13	0.76	1025	Partial	0.3663	Minor
		1026	Complete	0.0516	0.28
14	0.82	1027	Partial	0.3465	Minor
		1028	Complete	0.0352	0.19
15	0.87	1029	Partial	0.2808	Minor
		1030	Complete	0.0290	0.16
16	1.39	1031	Partial	0.2190	None
		1032	Complete	0.0145	0.08

*Equation 2 used to calculate pitting factor.

Table 5-2 Weight losses of coupons in container #2

Vessel number	Pitting Factor*	Coupon number	Level in vessel	mass loss (g)	Corrosion rate (mpy)
17	1.65	1033	Partial	0.1115	None
		1034	Complete	0.0043	0.02
18	1.80	1035	Partial	0.1118	None
		1036	Complete	0.0133	0.07
19	0.86	1037	Partial	0.3751	Minor
		1038	Complete	0.0389	0.21
20	0.91	1039	Partial	0.2185	Minor
		1040	Complete	0.0337	0.18
21	0.97	1041	Partial	0.1882	None
		1042	Complete	0.0170	0.09
22	1.12	1043	Partial	0.1008	None
		1044	Complete	0.0073	0.04
23	1.17	1045	Partial	0.1033	None
		1046	Complete	0.0316	0.17
24	1.33	1047	Partial	0.1040	None
		1048	Complete	0.0097	0.05
25	1.75	1051	Partial	0.0461	None
		1052	Complete	0.0057	0.03

*Equation 2 used to calculate pitting factor.

The pitting factor and the hydroxide ion concentration were utilized to assess the corrosion behavior further. Table 5-3 shows the results from the immersed coupons and indicates that the hydroxide concentration controls the degree of corrosion in the bulk solution. The corrosion rates were 1 mpy or less for hydroxide concentrations greater than 0.1 and decrease with an increase in hydroxide concentration. In general, an increase in the pitting factor, which is associated with an increase in the nitrite concentration, resulted in a decrease in the corrosion rate as well. Although for hydroxide concentrations of 0.1 M and greater, this decrease was relatively insignificant. These results indicate that for bulk solutions, if the hydroxide concentration is greater than 0.1 M, the degree of corrosion is relatively insignificant (i.e., 1 mpy or less) irrespective of the pitting factor.

Table 5-3 Results of completely immersed coupons based on hydroxide concentration.

Hydroxide (M)	Corrosion rates of Pitting Factor (mpy)		
	< 1	between 1 and 2	> 2
0.0001	2.04, 1.86	0.41, 0.33	0.30, 0.23
0.1	1.00, 0.18	0.17 - 0.44	N/A
0.3	0.16 - 0.37	0.02 - 0.08	N/A
0.6	0.09 - 0.21	0.03 - 0.17	N/A

Table 5-4 shows the results from the partially immersed coupons. The behavior at the LAI showed a stronger dependence on the pitting factor than was observed to the totally immersed coupons. These results indicate that for a pitting factor less than 1, minor or severe attack was observed for all hydroxide concentrations less than 0.6 M. For a pitting factor between 1 and 2, minor or no corrosion was observed for hydroxide concentrations greater than 0.3 M and greater. Additionally, at 0.1 M hydroxide, the addition of nitrite (0.6 M and 1.2 M) either reduced the amount of attack at the interface or eliminated it completely. Additional tests at either higher hydroxide concentrations (e.g., 1 M) or at pitting factors greater than 2 with hydroxide concentrations less than 0.1 M could further define the margin on LAI corrosion. It should be noted that tests at Savannah River indicate that for hydroxide concentrations greater than 1 M, attack at the liquid air interface is minimal, and therefore tests at these concentrations would not necessarily define the limits. Additionally, previous tests show that nitrite inhibition at lower pH, which correlates to a higher pitting factor may also be effective.

Table 5-4 Results of partially immersed coupons based on hydroxide concentration. The degree of corrosion at LAI is reported.

Hydroxide (M)	Degree of corrosion based on Pitting Factor		
	< 1	between 1 and 2	> 2
0.0001	Severe	Minor/None	Minor/None
0.1	Severe/None	Minor/None	N/A
0.3	None	None	N/A
0.6	Minor/None	None	N/A

Figure 5-1 shows the areas where LAI corrosion is potentially significant. The hydroxide concentration, represented in terms of pH, is plotted against the pitting factor. The red area represents areas where the coupons indicated severe or minor corrosion, while the green area represents areas where the coupons indicated essentially no corrosion. There was one result, Test 3, that was near the boundary, however, this again was only superficial attack. The plot shows regions of concern, in red, that are similar to what was observed based on the previous CPP tests [20].

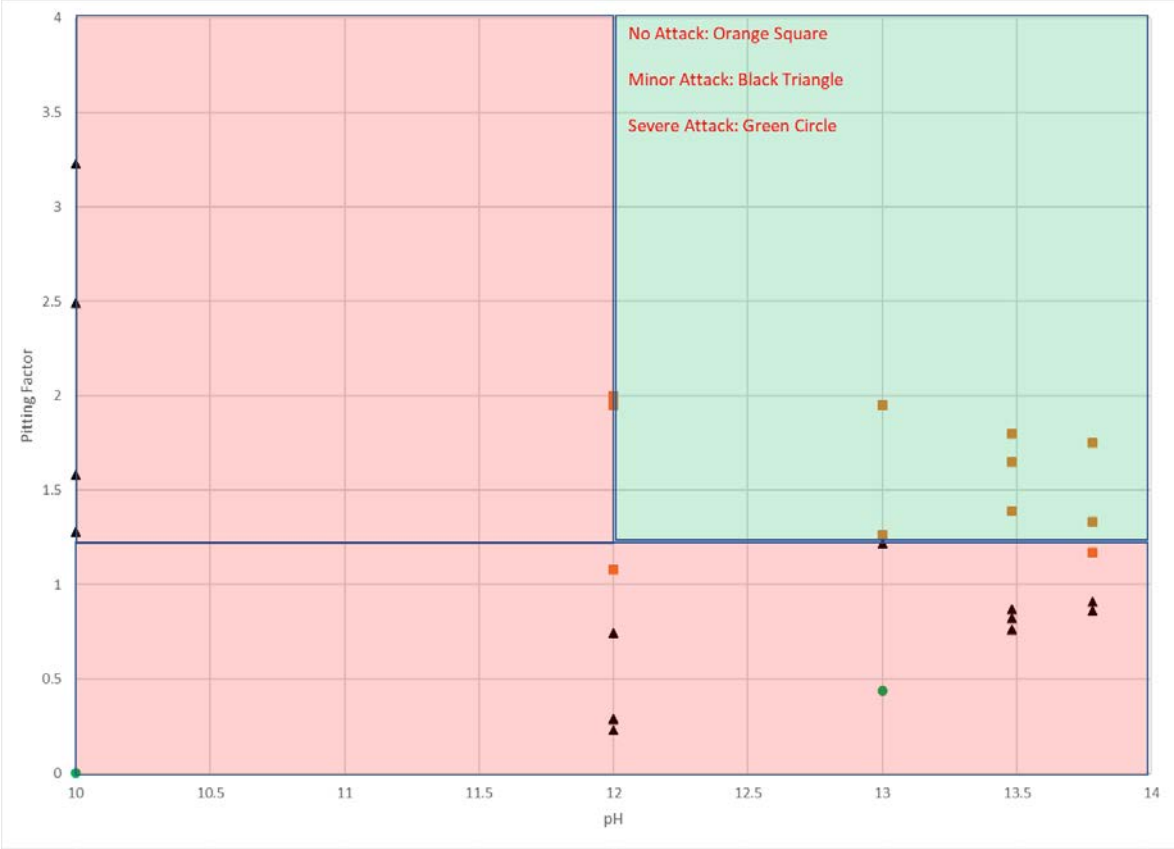

Figure 5-1 Chemistry envelope for liquid air interface corrosion based on coupon test results.

The OCP behavior for ten tests was examined (see Table 5-5). Figure 5-2 shows the OCP transients during the four months for these tests. The most active OCP was maintained at a range of -440 to -495 mV vs. SCE for Solution 1. Most of the OCP transients were maintained at a range of -200 to -400 mV vs. SCE. There were two instances in which the OCP started to drift in the noble potential direction, but after approximately 600 hours quickly shifted to more negative potentials and was in the same range as others (Solutions 5 and 11). All other OCP transients are shown in Appendix D.

Table 5-5 Selection of test conditions of New limits immersion tests for the discussion of results

Test	Hydroxide (M)	Nitrite (M)	Nitrate (M)	Chloride (M)	Sulfate (M)	TIC (M)	Pitting Factor
1	0.0001	0	0.153	0.049	0.2	0.1	7.65E-4
3	0.0001	0.6	0.154	0.050	0.2	0.1	1.28
5	0.0001	1.2	0.023	0.058	0.2	0.1	2.49
6	0.0001	1.2	0.797	0.005	0.2	0.1	3.23
9	0.1	0.6	0.452	0.073	0.2	0.1	1.22
11	0.1	1.2	0.076	0.094	0.2	0.1	1.95
13	0.3	0	0.715	0.135	0.2	0.1	0.76
18	0.3	1.2	2.201	0.042	0.2	0.1	1.80
21	0.6	0	2.444	0.144	0.2	0.1	0.97
25	0.6	1.2	4.224	0.018	0.2	0.1	1.75

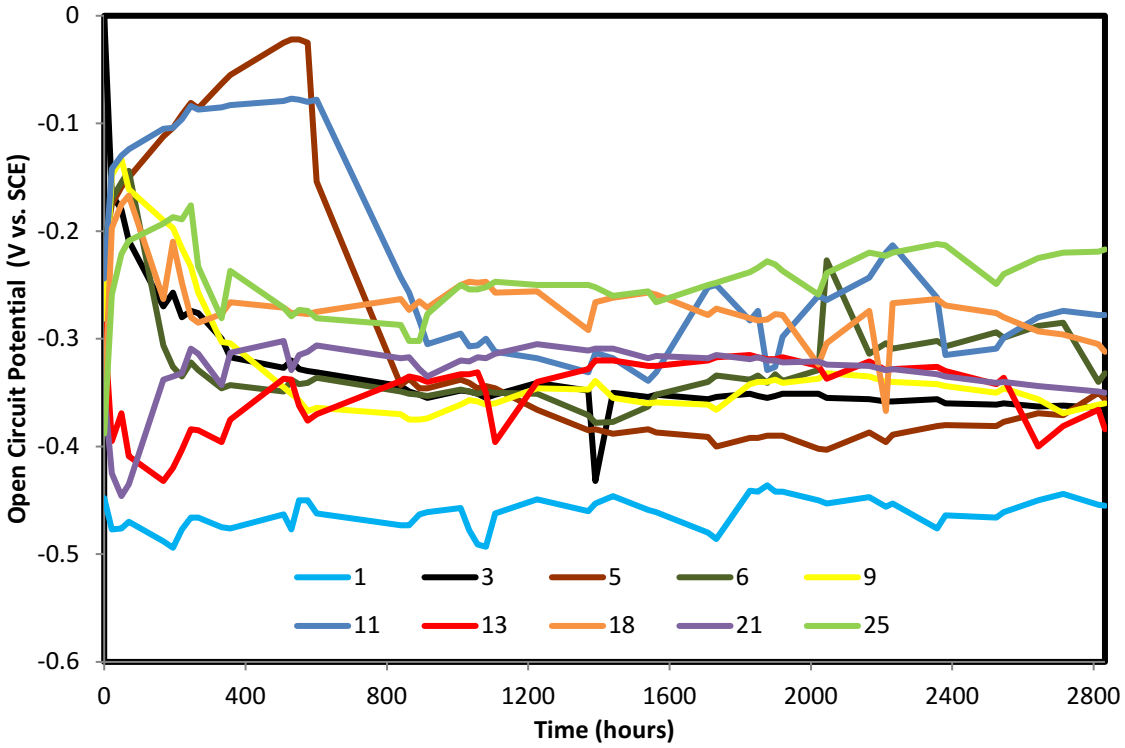

Figure 5-2 OCP transients versus time of completely immersed coupons in solution

Comparing pictures and 3-D measuring macroscope images, only coupons exposed in solution 1 and 2 showed significant pit depth around LAI after 4 months. The images are presented in Figure 5-3 . The measuring macroscope images indicate localized corrosion at the solution line and above with penetration depths at a range of 0.05 to 0.2 mm at minor deep areas and correspond to around 2.0 to 7.9 mils.

After test picture | After cleaning picture | Measuring macroscope image

(a)

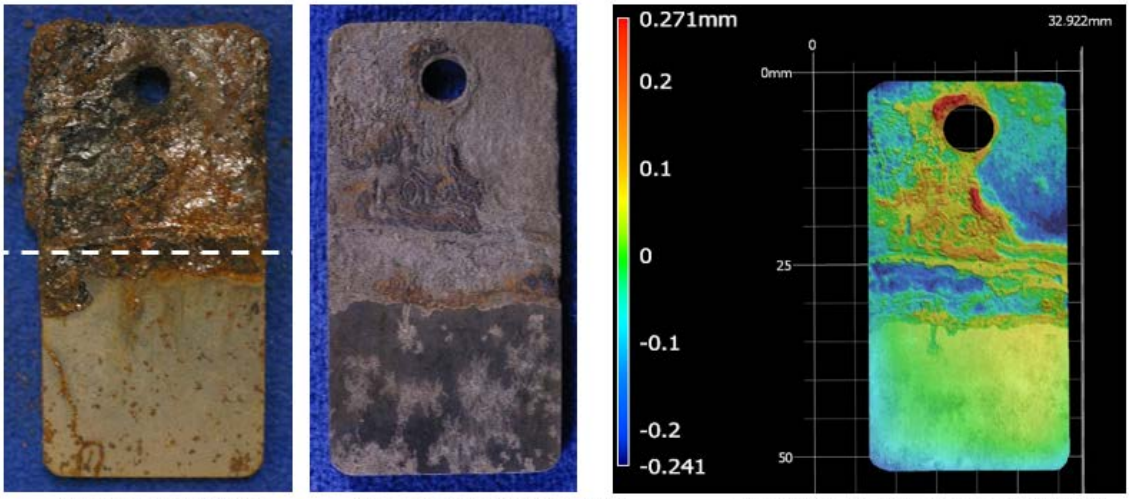

After test picture | After cleaning picture | Measuring macroscope image

(b)

Figure 5-3 Picture after test, after cleaning and 3-D measuring macroscope image of coupon 1001 (a) and coupon 1003 (b) exposed in Solution 1 and 2, respectively (engraving error for the carbon steel as A285).

Measuring macroscopic images for the coupons partially and completely immersed in solutions that presented the highest and lowest corrosion rates from the selected specimens for OCP comparison are displayed in Figure 5-4. Coupon 1001 was presented before and had the most aggressive attack of all coupons with two-thirds of the coupon corroded. Its counterpart, Coupon 1002, that was completely immersed presented deep pits around the mount with a maximum depth

of 0.31 mm (12.2 mils) on the upper right side and shallow general attack at the lower left side with a range of depth of 0.1 to 0.2 mm (3.9 to 7.9 to mils). The coupons immersed in solution 25 (i.e., coupon 1051 and 1052) showed no signs of corrosion with only a shallow region corresponded to VSC at the upper right corner of coupon 1051 with maximum depths of 0.05 mm (2.0 mils). Pit depths for all the remaining coupons in immersed areas were all less than 1 mil. The long term corrosion test showed that the combination of pitting factor can help predict the corrosive environment to some extent, but additional measures such as maintaining a high hydroxide concentration in the solution are critical for corrosion inhibition of carbon steel.

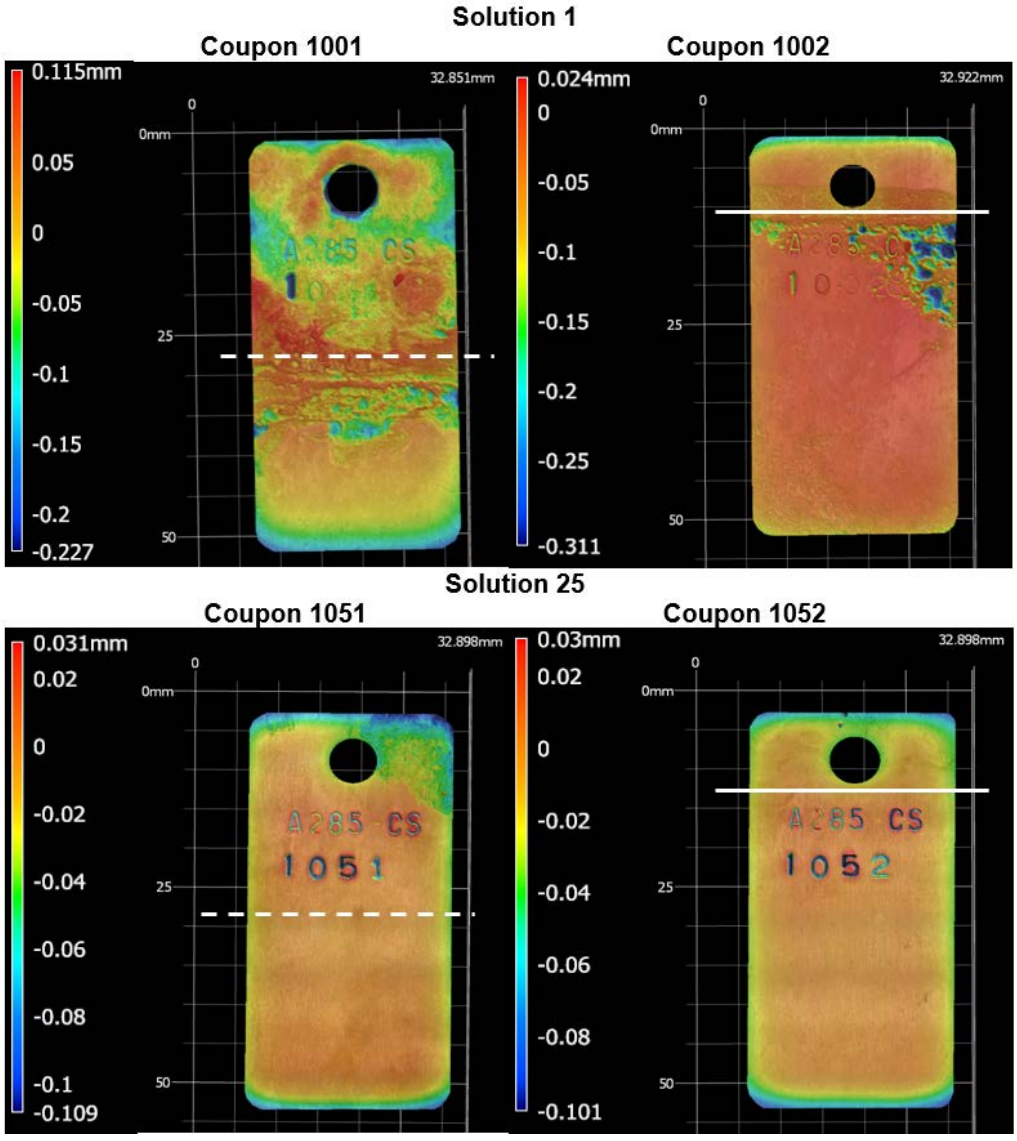

Figure 5-4: Measuring macroscope images of partial and complete immersed coupons for highest and lowest corrosion rates obtained from selected coupons (engraving error for the carbon steel as A285).

5.1.2 Electrochemical Tests

Electrochemical testing continued in FY18 to test the pitting factor in borderline conditions in simple simulants and tank chemistry simulants. The pitting factor, as described in more detail in previous reports [5], helps in targeting pitting corrosion susceptibility for specific chemistries of significant components in the waste. Testing primarily at pitting factors between 1 and 2 showed borderline conditions that we wanted to address to determine the competency to predict pass or fail categorization.

The logistic approach was adopted again for the analysis. The "pass" or "fail" condition was determined from the six categories specified by the pitting test protocol. More information on the categories can be found elsewhere [16]. Categories 1 and 2 were assigned a "0" or pass rating, while categories 4, 5, and 6 were assigned a "1" or fail rating. A category 3, or mixed hysteresis condition that was considered inconclusive, was re-tested using the modified ASTM G192 test method [17]. The ASTM G192 method is based on the Tsujikawa-Hisamatsu Electrochemical (THE) method derived from the two Japanese researchers that developed the technique [18] and can be used to determine repassivation potentials. In this case, it was used to provide a definite categorization of pass or fail for borderline cases that showed mixed hysteresis by using a modified version developed by DNV-GL [19]. If the result was a pass, "0" was used and if it was a fail "1" was used.
Borderline conditions were observed in cases where pitting factor is between 1 and 2 and/or in most of the CPP results which resulted in mixed hysteresis. Because of the mixed hysteresis, it is difficult to assign a pass or fail criterion and a modified ASTM G192 test was performed as a result. To investigate this range, fifteen tests were selected with the corresponding pitting factors between 1 and 2 and greater than 2, and hydroxide concentrations from 0.0001 M (i.e., pH 10) to 0.6 M. The response in CPP tests and results are summarized in Table 5-6. As before, the modified G192 test was utilized to interpret the mixed hysteresis result to determine if a condition was a pass.

Table 5-6 Test conditions and results of testing from selected test with pitting factors between 1 and 2 and above

Test	Temp. (°C)	Target pH	Pitting Factor	Category		Pitting on sample		Repassivation Potential (mV vs. SCE)			Logistic Approach
				run 1	run 2	run 1	run 2	run 1	run 2	modified G192	
1	35	10	1.33	3	5	Yes	Yes	N/A	N/A	595	0
2	35	10	2.95	5	5	Yes	Yes	N/A	N/A	238	0
3	35	10	1.45	1	3	No	Yes	N/A	N/A	489	0
4	35	>12	1.44	1	4	No	Yes	N/A	-178	Not found	1
5	35	>12	1.56	1	2	No	Yes	N/A	443	471	0
6	35	>12	2.53	1	3	No	No	N/A	547	531	0
7	35	>12	1.44	2	3	No	Yes	13	N/A	530	0
8	35	>12	1.53	1	1	No	No	N/A	N/A	No	0
9	35	>12	1.97	2	2	Yes	Yes	409	341	No	0
10	35	>12	1.58	1	1	No	Yes	N/A	N/A	No	0
11	35	>12	1.57	3	3	No	No	N/A	N/A	493	0
12	35	>12	3.24	3	3	Yes	No	N/A	N/A	235	0
13	35	>12	1.34	2	2	Yes	Yes	221	370	No	0
14	35	>12	1.36	1	1	No	No	N/A	N/A	No	0
15	35	>12	1.41	3	1	Yes	No	N/A	N/A	445	0
16	35	>12	1.95	1	1	No	No	N/A	N/A	No	0
17	35	>12	1.67	3	3	No	No	N/A	N/A	349	0
18	35	>12	2.33	1	1	No	No	N/A	N/A	No	0
19	35	>12	2.33	1	1	No	No	N/A	N/A	No	0
20	35	>12	1.75	1	1	No	No	N/A	N/A	No	0
21	35	>12	1.29	1	1	No	No	N/A	N/A	No	0
22	35	>12	1.29	1	1	No	No	N/A	N/A	No	0
23	35	>12	7.49	1	1	No	No	N/A	N/A	No	0

For tests between pitting factors 1 and 2 and slightly above, seven of the fifteen results showed mixed hysteresis. Also, seven of the fifteen tests resulted in samples that pitted and did not pit during duplicate runs. All the tank chemistries showed a pass with negative hysteresis (category 1) except Test 17 that showed mixed hysteresis (category 3). After running modified ASTM G192 tests, most of the tests showed a passing category with just one fail. Even though, the use of a modified ASTM G192 test was needed for determination of pass or fail, it seems that for pitting factor higher than 1, a pass is the most likely response with above 93% of success for the 15 tests performed, except for Test 4 in which one test passed and the duplicate barely failed. The simulant contained no nitrite and thus verifies the need to include a minimum required nitrite in order to minimize the risk of pitting. A minimum of 0.2 M nitrite will be specified.

To study the fluoride effects and separate the halide effects of chloride and fluoride in the pitting factor equation, fifteen tests were statistically selected for electrochemical experiments. Historical CPP data with fluoride was analyzed with approximately 110 data points. It was recommended an additional 15 tests with 8 different conditions to achieve a balanced design. Figure 5-5 shows the scatterplot with the proposed tests in purple triangles. The compositions were listed in the experimental section shown in Table 4-4.

Table **5-7** lists the response for CPP as well as the observations of pitting and no pitting. The concentration of fluoride species was included because of changes in concentration needed for solubility of species into solution. By adjusting the fluoride additions at the end with small quantities, the fluoride concentration that was soluble was recorded and if precipitation started to occur more additions of fluoride were halted. The highlighted values correspond to new concentration of fluoride in solution.

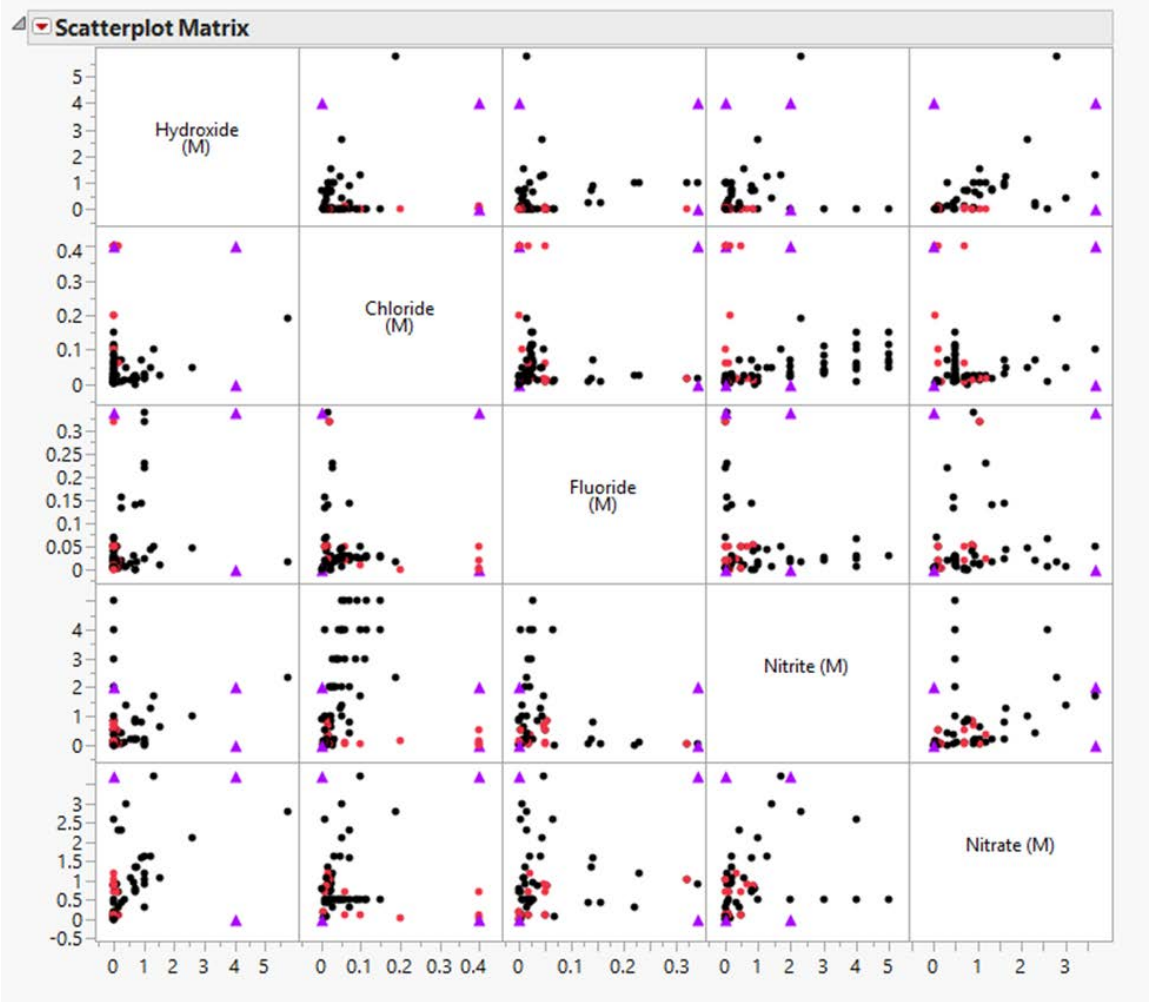

Figure 5-5 Scatterplot showing the present data points and new proposed tests (purple triangles)

Table 5-7 Test conditions and results of testing from statistically design tests to investigate fluoride effects

Test	Temp. (°C)	Fluoride (M)	Target pH	Pitting Factor	Category	Pitting on sample	Repassivation potential (mV vs. SCE)	Logistic Approach
1	35	0.02	>12	2.84	1	No	N/A	0
2	35	0.02	>12	2.84	1	No	N/A	0
3	35	0.3	10	0.27	5	Yes	N/A	1
4	35	0.3	10	0.27	4	Yes	-167	1
5	35	0	>12	2.88	1	No	N/A	0
6	35	0	>12	2.88	1	No	N/A	0
7	35	0.3	>12	6.62	1	Yes	N/A	0
8	35	0.26	>12	6.62	1	Yes	N/A	0
9	35	0.14	>12	3.45	1	Yes	N/A	0
10	35	0	>12	N/A	1	No	N/A	0
11	35	0	>12	2.88	1	No	N/A	0
12	35	0	>12	9.73	1	No	N/A	0
13	35	0.3	10	0.27	4	Yes	-161	1
14	35	0.3	10	0.27	4	Yes	-180	1
15	35	0.22	>12	2.48	1	No	N/A	0

From the fifteen tests, ten showed negative hysteresis (category 1) consistent with a pass. One case showed positive hysteresis (category 5) and three showed closed looped positive hysteresis less than 200 mV vs OCP (category 4) consistent with a failed condition. For this test, all the conditions matched the pitting factor prediction.

Logistic regression was performed with the results of pitting factor between 1 and 2 and fluoride effects (Table 5-6 and Table 5-7, respectively). The resulting linear equation with coefficients is presented below (Equation 3),

$$Lin(0)= 1.99 + 15.54\,[OH^-] + 2.99\,[NO_2^-] - 1.93\,[NO_3^-] - 32.11\,[Cl^-] - 10.7\,[F^-] \quad \textbf{Equation 3}$$

The coefficients were added into the pitting factor and the resulting equation with the specific contributions of fluoride and chloride is shown in Equation 4. The contribution of chloride for the equation is around 3 times more significant than fluoride.

$$\text{Pitting Factor} = \frac{\text{Inhibitor Species}}{\text{Aggressive Species}} = \frac{8.06\,[OH^-]+1.55\,[NO_2^-]}{[NO_3^-]+16.7\,[Cl^-]+5.7\,[Fl^-]} \quad \textbf{Equation 4}$$

The pitting factor equation obtained was used to establish new corrosion control limits recommended for DSTs. The equation was validated with model simulations and comparison with historical results. The results were compiled in a report that is currently in draft form to be submitted to WRPS [20] summarizing the technical basis for the recommended changes in the chemistry controls.

5.2 Secondary Liner Corrosion Studies

FY18 experiments were conducted with the GW simulant because FY17 studies indicated that GW simulant was more corrosive than LDP simulant. In addition to coupons, ER probes were used to continuously assess the corrosion environment and effect of VCIs. The ER probes were placed at Level 1 positions. In using ER probes, corrosion rates are obtained by measuring resistance of the probe element, which changes over time, as metal loss occurs. The reduction in cross-sectional area of the element, fabricated of 1080 carbon steel, will cause an increase in electrical resistance as it corrodes.

In FY17 studies, the VCIs were applied to coupons by dipping the coupons in a VCI chemistry for certain period. For this year's studies, the VCIs were applied by adding the VCIs directly to the solution. Another test was conducted by adding $CaCO_3$ to the GW solution. The test was to simulate contact of an aged concrete with GW, and the effect of the resulting solution on corrosion of secondary liner.

VCIs were directly added to the GW simulant. Experiments were conducted using the vessels described in section 4.3.3. The VCIs' dosages were as per the manufacturer's recommendation (Cortec®). The ER probes were placed in the vessels; with one ER probe immersed in the solution and another one at Level 1 in each vessel. The ER probe data and corresponding corrosion rates are presented in Figure 5-6 and Figure 5-7 for VCI-A and VCI-B respectively.

ER probe data and corresponding corrosion rates for GW + VCI-A are presented in Figure 5-6(a). The data points are presented by filled circles, and corrosion rates by solid lines. The data for immersed and vapor space ER probes are in blue and orange, respectively. Figure 5-6(b) and Figure 5-6(c) have images of the ER probes taken immediately after completing the experiment. Figure 5-6(b) shows image of the ER probe that was immersed in the test solution, i.e., GW + VCI-A, for the duration of the experiment. The probe image is shiny and shows no signs of corrosion. The probe image is consistent with the immersed ER probe data in Figure 5-6(a). Figure 5-6(c) shows image of the ER probe that was in vapor space of the test solution. The ER probe wire loop in Figure 5-6(c) shows visible signs of corrosion; analysis of this ER data yielded corrosion rate of 2 mpy; the ER probe image and calculated corrosion rates are qualitatively consistent with each other.

ER probe data and corresponding corrosion rates for GW + VCI-B are presented in Figure 5-7(a), with measured data points represented by filled circles, and calculated corrosion rates by solid lines. The data for immersed and vapor space ER probes are in blue and orange colors, respectively. Figure 5-7(b) and Figure 5-7(c) have images of the ER probes taken immediately after completing the experiment. Figure 5-7(b) shows image of the ER probe that was immersed in the test solution, i.e., GW + VCI-B, for the duration of the experiment. The probe image is shiny and shows no signs of corrosion. The probe image is consistent with the immersed ER probe data in Figure 5-7(a). Figure 5-7(c) shows image of the ER probe that was in vapor space of the test solution. The probe wire loop in Figure 5-7(c) also shows no visible signs of corrosion; consistent with the ER probe data in Figure 5-7(c).

Several coupons were placed in each experimental setup and were extracted after completion. Images of the coupons exposed to GW + VCI-A environment are presented in Figure 5-8. The images also include photographs of test solution samples collected after completion of the experiment. It was observed that a yellowish-brown substance precipitated at the bottom of the test

vessel. Images of the test solution during the test, and samples of the test solution are shown in Figure 5-8. A sample of the test solution from bottom of the test vessel was collected and is shown in Figure 5-8(h). Additional analysis will be conducted to determine composition and cause of precipitated substance.

Images of the coupons exposed to GW + VCI-B environment are presented in Figure 5-9. The images also include photographs of test solution samples collected after completion of the experiment. It was observed that a white substance precipitated out and floated on top of the test vessel. In addition, a yellowish-brown substance precipitated at the bottom of the test vessel. Images of the test solution during the test, and samples of the test solution are shown in Figure 5-9. A sample of the white substance was collected in a vial and is shown in Figure 5-9(g). In addition, test solution from bottom of the test vessel was collected and is shown in Figure 5-9(h). Additional analysis will be conducted to determine composition and cause of precipitated substances.

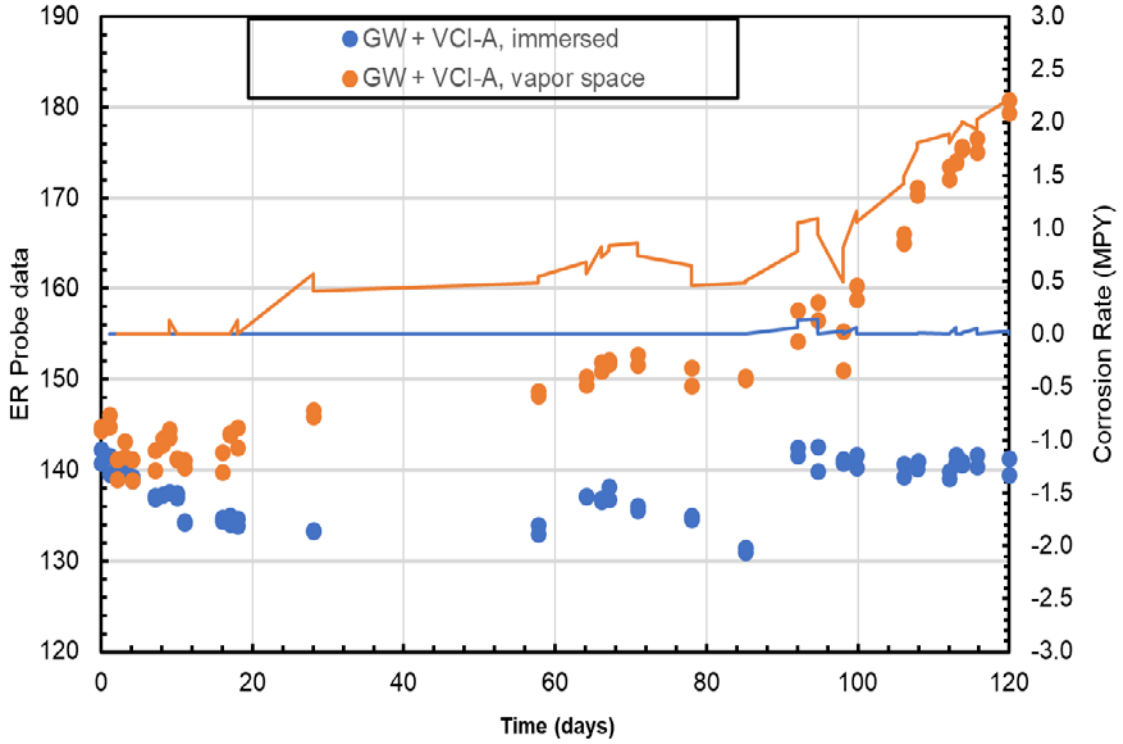

(a) ER Probe Data and Corrosion Rates

(b) ER probe immersed in the solution

(c) ER probe in the vapor space

Figure 5-6 (a) VCI-A (VpCI-337) experiment ER probe data, and corresponding corrosion rates. Filled circles are the ER probe measurements and solid lines represent the corrosion rates. Images of the ER Probes After Completing the Experiment: (b) Probe that was Immersed in Solution, (c) Probe that was Placed in Vapor Space of the Experimental Setup

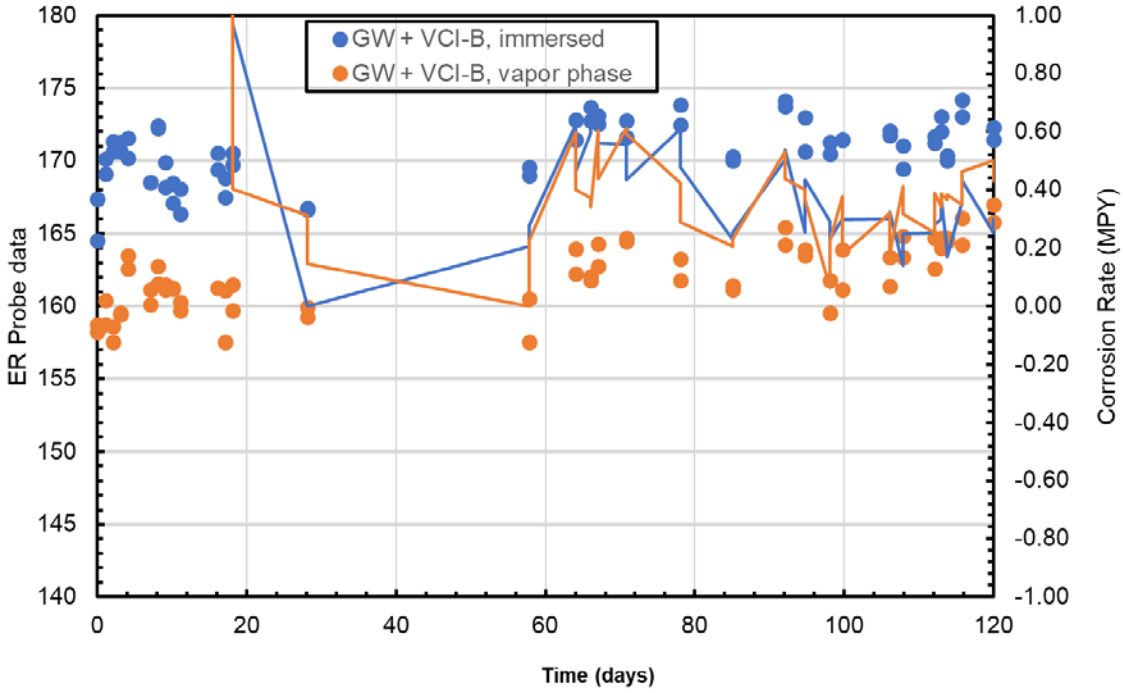

(a) ER Probe Data and Corrosion Rates

(b) Immersed ER probe

(c) Vapor Space ER probe

Figure 5-7 (a) VCI-B (VpCI-609 + VpCI-645) experiment ER probe data, and corresponding corrosion rates. Filled circles are the ER probe measurements and solid lines represent the corrosion rates. Images of the ER Probes After Completing the Experiment: (b) Probe that was Immersed in Solution, (c) Probe that was Placed in Vapor Space of the Setup

(a) Level 3 GW + VCI-A Coupons

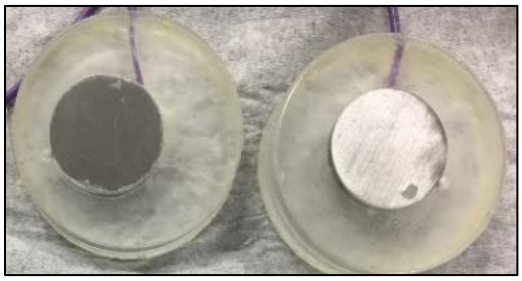

(b) Level 2 GW + VCI-A Coupons

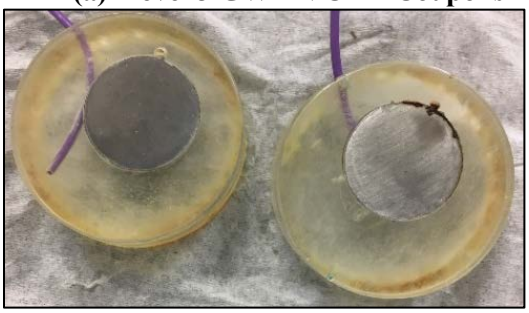

(c) Level 1 GW + VCI-A Coupons

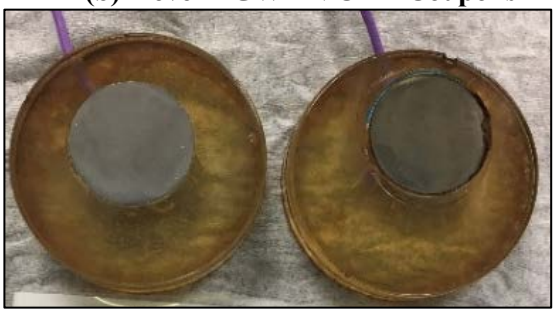

(d) Immersed GW + VCI-A Coupons

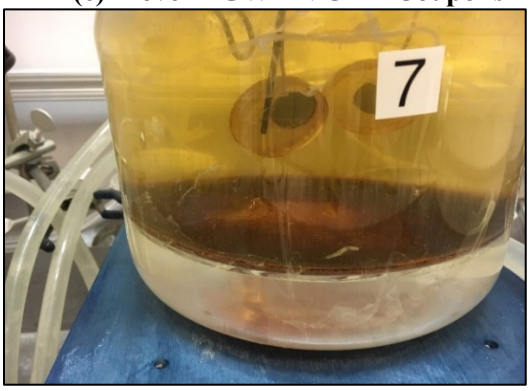

(e) Test Solution During Experiment

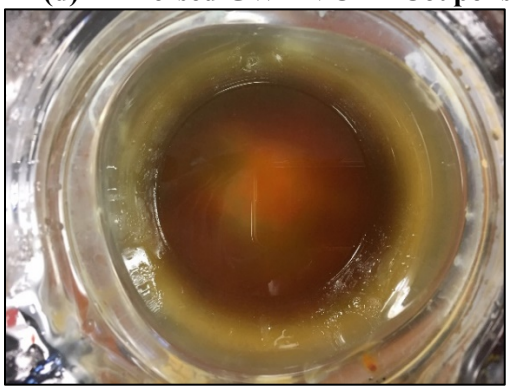

(f) Test Solution After Experiment

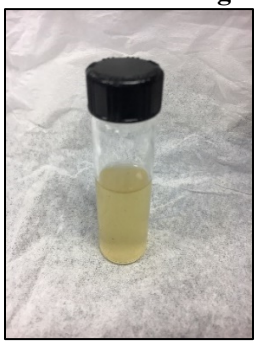

(g) Test solution without precipitates

(h) Test solution with precipitated substance

Figure 5-8 Images of the Post-test Coupons and Test Solution for GW + VCI-A

(a) Level 3 GW + VCI-B Coupons

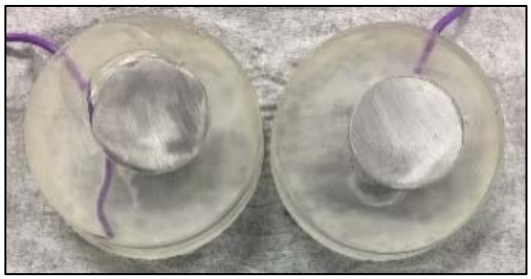

(b) Level 2 GW + VCI-B Coupons

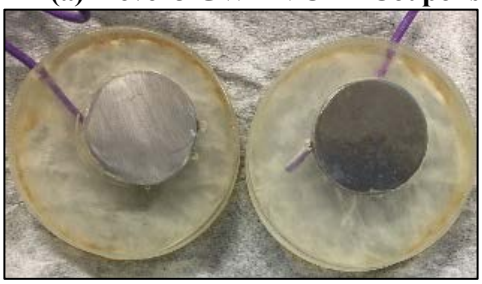

(c) Level 1 GW + VCI-B Coupons

(d) Immersed GW + VCI-B Coupons

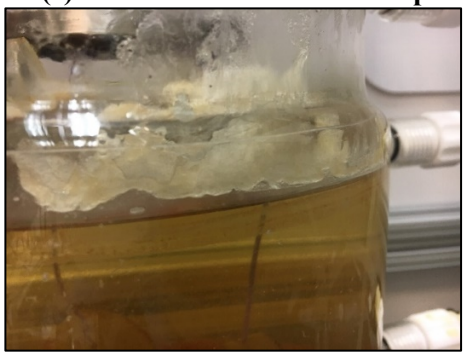

(e) Test Solution with Focus on White Floating Substance

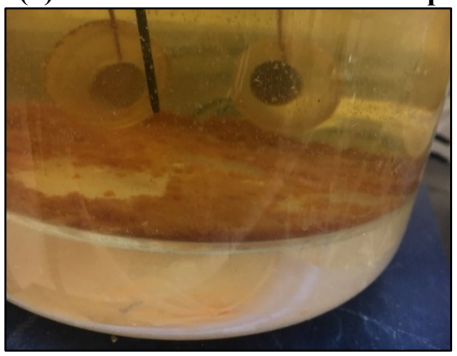

(f) Test Solution with Focus on Precipitants

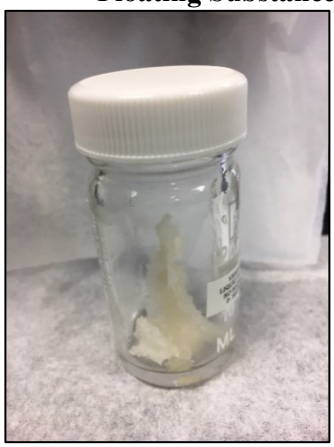

(g) Sample of White floating substance

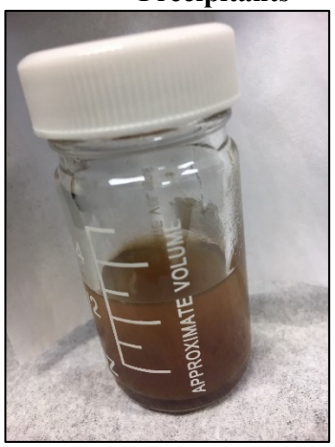

(h) Sample of test solution with precipitated substance

Figure 5-9 Images of the Post-test Coupons and Test Solution for GW + VCI-B

Images of the GW + $CaCO_3$ coupons are presented in Figure 5-10. Several coupons experienced extensive corrosion. Coupons were cleaned with Clarke's solution to remove corrosion products and measure accurate mass losses. Several coupons exhibited patch and pitting corrosion. Those coupons were surface profiled using a 3-D measuring microscope. Images and surface contours of those coupons are presented in Figure 5-11. The mass-loss and surface profile data were used to estimate corrosion rates. The mass-loss data were used to estimate surface average corrosion rates. The surface profile data were used to identify maximum pit depth which was then used to estimate the pitting rate by normalizing the pit depth on an annual basis. The corrosion rate data is listed in Table 5-8.

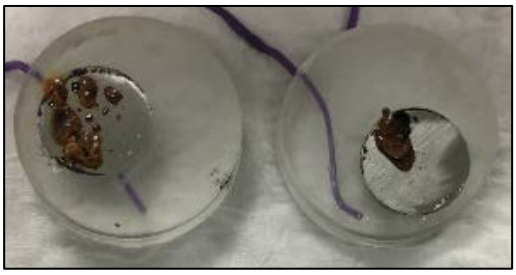

(a) Level 3 GW + $CaCO_3$ Coupons

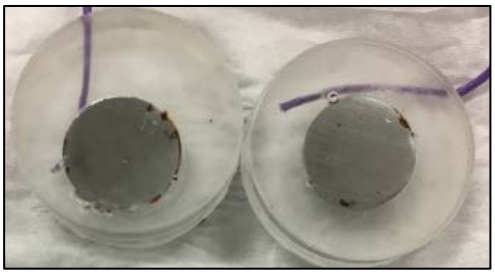

(b) Level 2 GW + $CaCO_3$ Coupons

(c) Level 1 GW + $CaCO_3$ Coupons

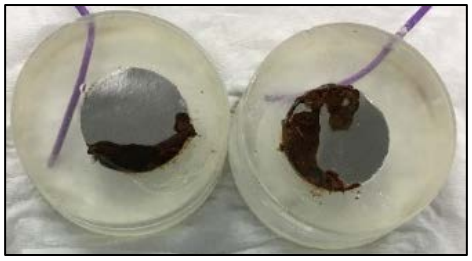

(d) Immersed GW + $CaCO_3$ Coupons

Figure 5-10 Images of the coupons in GW + $CaCO_3$ experimental setup

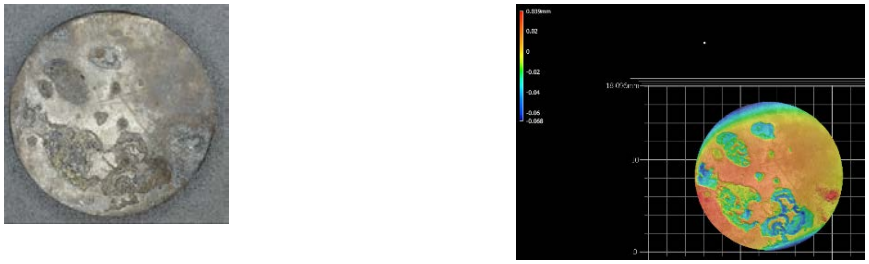

Coupon 1 (GW + $CaCO_3$ Level 3)

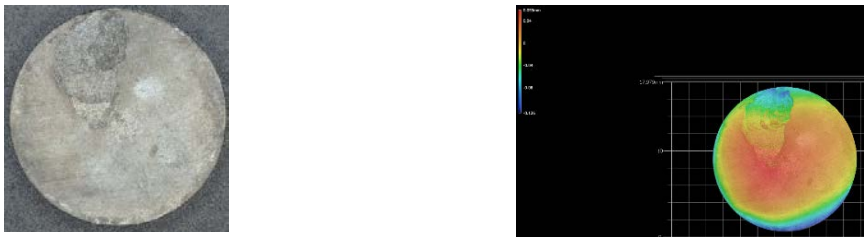

Coupon 2 (GW + $CaCO_3$ Level 3)

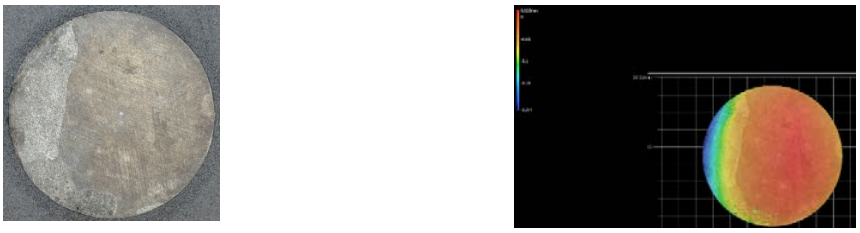

Coupon 7 (GW + $CaCO_3$ immersed)

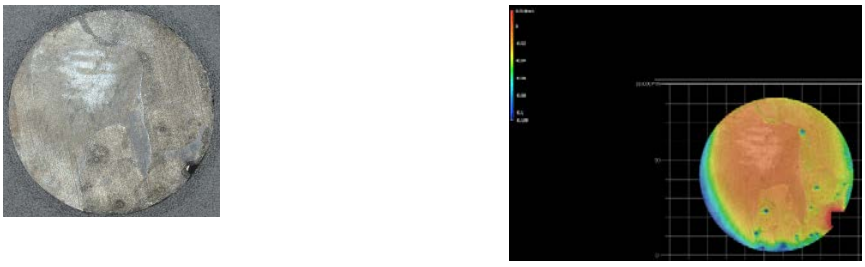

Coupon 8 (GW + $CaCO_3$ immersed)

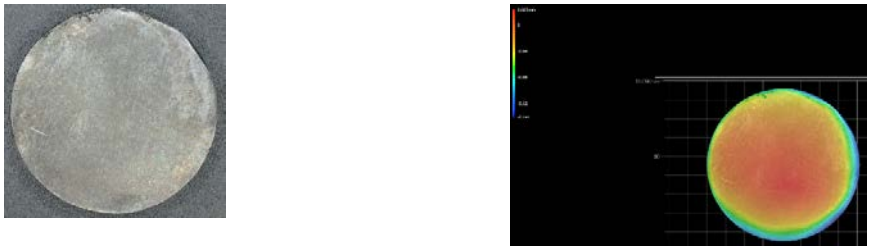

Coupon 14 (GW + VCI-A Level 1)

Figure 5-11 Images and surface profiles of selected coupons

Table 5-8 Corrosion rates estimated using the coupons

Test solution	Coupon number	Coupon location	Initial mass (g)	mass loss (g)	Mass-Loss Based Corrosion rate (mpy)	Pitting Corrosion Rate (mpy)
GW+ $CaCO_3$	1	High (Level3)	4.4201	4.4026	1.44	8.0
	2	High (Level3)	4.4334	4.4242	0.76	10.0
	3	Middle (Level 2)	4.6825	4.6816	0.07	-
	4	Middle (Level 2)	4.6199	4.6172	0.22	-
	5	Low (Level 1)	4.8542	4.8535	0.06	-
	6	Low (Level 1)	4.7659	4.7638	0.17	-
	7	Immersed	4.6835	4.6772	0.52	13.2
	8	Immersed	4.1612	4.1498	0.94	13.0
GW + VCI-A	9	High (Level3)	4.3888	4.388	0.07	-
	10	High (Level3)	4.5731	4.5735	-0.03	-
	11	Middle (Level 2)	4.0665	4.0666	-0.01	-
	12	Middle (Level 2)	4.8176	4.81735	0.02	-
	13	Low (Level 1)	4.8273	4.82825	-0.08	-
	14	Low (Level 1)	4.2397	4.239	0.06	9.4
	15	Immersed	4.7021	4.701	0.09	-
	16	Immersed	4.8038	4.7979	0.49	-
GW + VCI-B	17	High (Level3)	4.0881	4.0881	0.00	-
	18	High (Level3)	4.5295	4.53	-0.04	-
	19	Middle (Level 2)	4.6435	4.6437	-0.02	-
	20	Middle (Level 2)	4.7884	4.7883	0.01	-
	21	Low (Level 1)	4.4266	4.4259	0.06	-
	22	Low (Level 1)	4.2499	4.25025	-0.03	-
	23	Immersed	4.3880	4.3871	0.07	-
	24	Immersed	4.1481	4.147	0.09	-

The mass-loss based and pitting corrosion rate data in Table 5-8 indicate that both VCI-A and VCI-B are effective in mitigating corrosion. The data indicate that GW + $CaCO_3$ is not as effective as VCIs in mitigating corrosion. The data also tends to support that VCI-B is more effective in mitigation corrosion compared to VCI-A: one coupon in VCI-A experimental setup experienced pitting corrosion rate of 9.4 mpy where no coupon in GW + VCI-B environment experienced pitting corrosion. Although, more studies are needed to support a valid conclusion for efficacy between the two formulations.

The issue of solid formation, i.e., precipitates, was investigated. The precipitates in the bottom of the test vessel in Figures 5-9(f), 5-9(h), 5-10(f), 5-10(h) are due to formation of ferric hydroxide. GW simulant chemistry is prepared by adding ferric chloride and ferric sulphate. Addition of ferric chloride and ferric sulphate to water results in formation of ferric hydroxide which has very low solubility: this explains the bottom precipitates in the four figures. The floating precipitates in Figures 5-10(e), and 5-10(g) are due the VCI chemistry. The finding has been discussed with the VCI vendor. A different concentration of similar VCI products will be tested in FY19 studies to prevent formation of floating precipitates.

5.3 Anodic Drift Studies

Initial CPP Measurements: Initial CPP data for two separate "bullet' coupons are presented in Figure 5-12 and corresponds to AN-107 simulant. As seen in the figure, the CPP curves have mixed hysteresis, i.e., a clear delineation between pitting and no-pitting cannot be made. Both forward and return curves in the CPP data for the two measurements overlap, indicating that CPP curves are inconclusive. Images of the bullet coupons immediately after the CPP tests are presented in Figure 5-13. As seen in Figure 5-13(a) and Figure 5-13(c), coupons' surfaces developed coloration with tints of purple, green, and blue, but tiny micro-pits were observed at high magnification at the coupon surface.

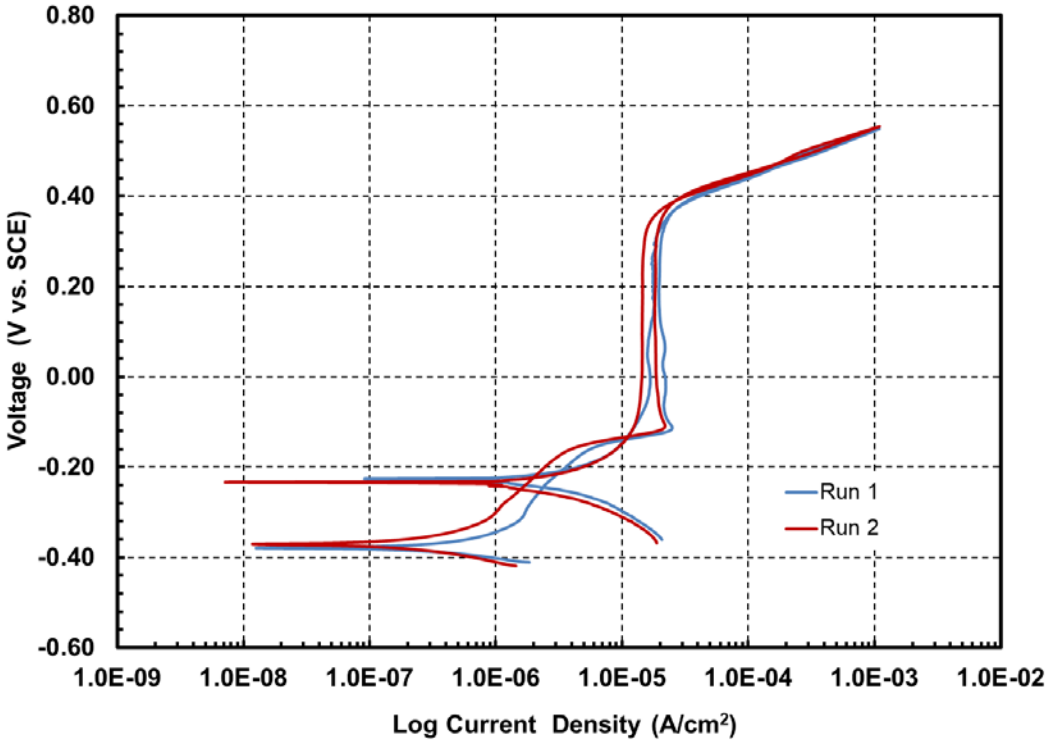

Figure 5-12 CPP data for the bullet coupon

(a) Run 1 coupon side image

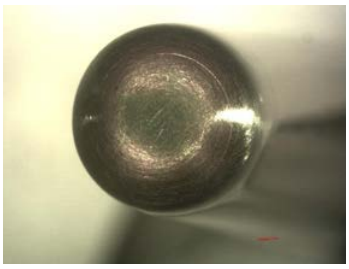

(b) Run 1 coupon nose image

(c) Run 2 coupon side image

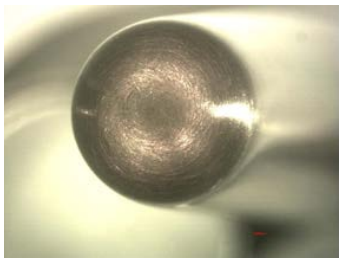

(d) Run 2 coupon side image

Figure 5-13 Images of the bullet coupons immediately after CPP tests

CPP data in Figure 5-12were collected using a separate set of experiments. Another set of experiments were setup to measure OCP drift, and Electrochemical Impedance Spectroscopy and CPP followed by OCP drift.

OCP Drift: The OCP data for the three coupons were collected for 120 days. The data for the bullet coupon are presented in Figure 5-14. As in the figure, the initial OCP is approximately -500 mV_{SCE}. The potential quickly rose to -320 mV and then stabilized at around -310 mV after several days.

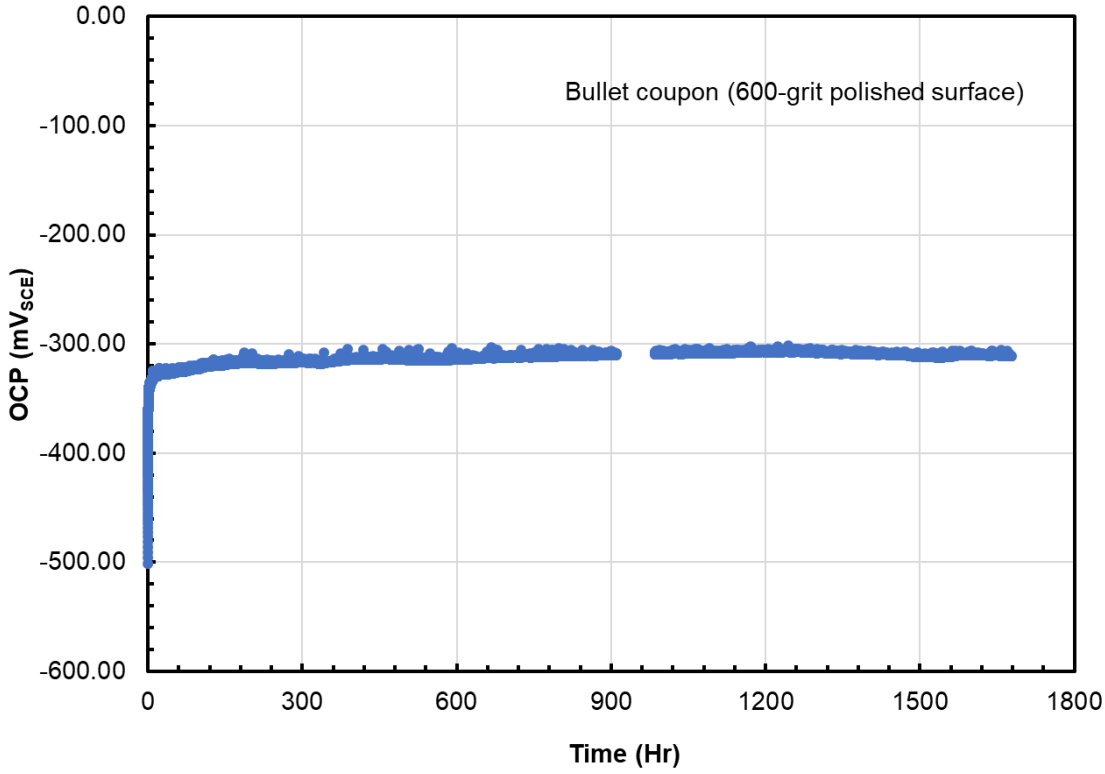

Figure 5-14 OCP data for the bullet coupon (600-grit ground surface)

OCP data for the mill-scale and partial mill-scale coupons are presented in Figure 5-15(a) and Figure 5-15(b), respectively. In Figure 5-15(b) data for the two coupons have been superimposed for comparison. As seen in Figure 5-15(a) and Figure 5-15(b), the OCP data for the coupons with pre-existing surface conditions such as mill-scale and corrosion products differed significantly compared to the bullet coupons with 600-grit ground surface. One of the key differences is the starting point for the OCP data. In Figure 5-14, the starting OCP value was more cathodic compared to the steady-state value. On other hand, terminal values of the OCPs are more cathodic compared to the initial values for mill- and partial mill-scale coupons. This indicate that the drift in OCP could either be cathodic or anodic, depending on the surface condition.

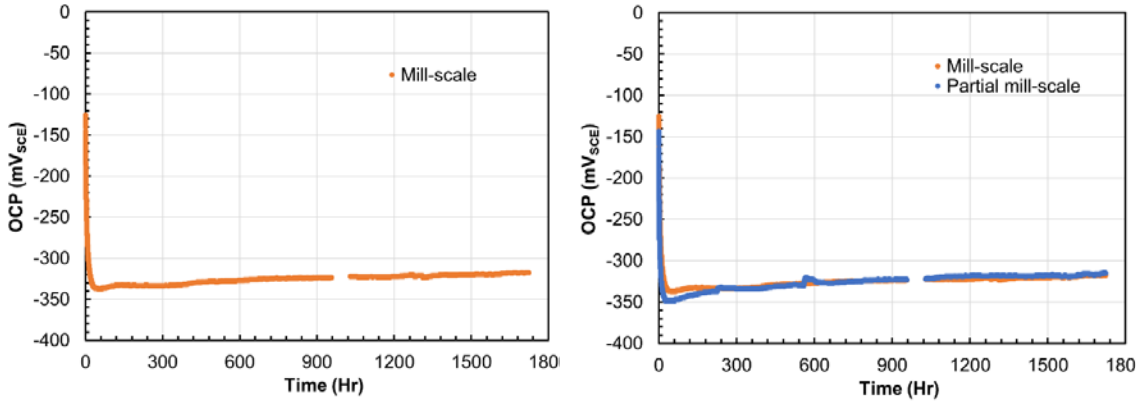

(a) OCP data for mill-scale coupon

(b) OCP data for mill- and partial mill-scale coupons

Figure 5-15 OCP data for the mill- and partial mill-scale coupons

Magnitude of the drift as a function of time is highlighted. OCP data at several time instances are listed in Table 5-9, including terminal values. The OCP drift for the bullet coupon is 180 mV, with 139 mV of the drift occurring in the first 2 hours. The OCP drift for the mill-scale coupon is 192 mV, with only 87 mV drift in the first two hours compared to 139 out of 180 mV for the bullet coupon. Similarly, partial mill-scale coupon's OCP drifted by 172 mV, with 115 mV drift in the first two hours. Another point is that the terminal OCPs of the three coupons are within 10 mV of each other, indicating that terminal values are somewhat independent of the initial surface condition.

Table 5-9 OCPs of the three coupons at several time instances

Time After Start (hr)	Bullet Coupon OCP (mV_{SCE})	Mill-Scale Coupon OCP (mV_{SCE})	Partial Mill-Scale Coupon OCP (mV_{SCE})
0	-501.1	-125.5	-143.3
2	-340.6	-212.5	-258.6
24	-327.0	-329.2	-346.1
48	-323.9	-337.1	-348.2
72	-321.4	-336.0	-347.0
Terminal	-311.1 (at 1677 hr)	-317.7 (at 1722 hr)	-315.1 (at 1722 hr)

Electrochemical Impedance Spectroscopy: Electrochemical Impedance Spectroscopy (EIS) was conducted on the three coupons. Bode plot of EIS data for the bullet coupon is presented in Figure 5-16(a). The data were collected in three runs; first two runs frequency range spanned from 10^{-4} to 2.5×10^{4} Hz, and third run frequency range spanned from 10^{-5} to 10^{4} Hz. As seen in Figure 5-16(a), the low frequency end, i.e., around 10^{-5} Hz, of the data reached steady-state, indicating that low frequency impedance is the polarization resistance. An electrical circuit model was fitted to the impedance data. The circuit model consisted of solution resistance, polarization resistance,

and constant phase element. Layout of the circuit model is shown in Figure 5-17. Circuit model fit to the bullet coupon's impedance data is shown in Figure 5-16(b).

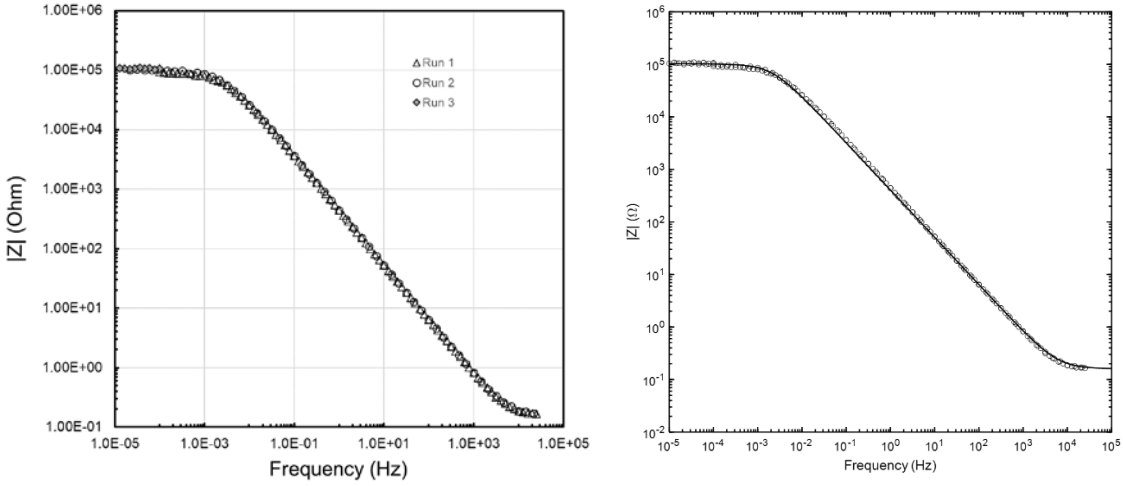

(a) EIS Data **(b) Circuit model fit to EIS data**

Figure 5-16 Bode Plot of Bullet Coupon (a) EIS Data and (b) Circuit Model Fit to EIS Data

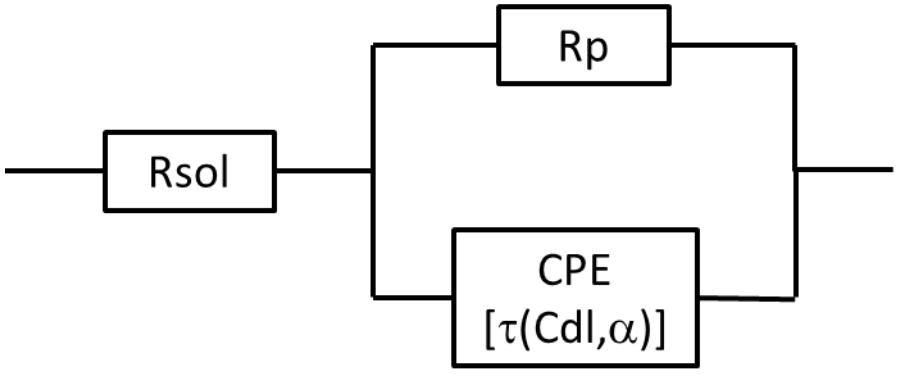

Figure 5-17 Equivalent Electrical Circuit Model

Bode plots of EIS data for the partial mill-scale and mill-scale coupons are presented in Figure 5-18(a) and Figure 5-19(a), respectively. The data for the two coupons were also collected in three separate runs; first two runs frequency range spanned from 10^{-4} to 2.5×10^{4} Hz, and third run frequency range spanned from 10^{-5} to 10^{4} Hz. The low frequency impedance of the two coupons did not reach steady-state, as seen in Figure 5-18(a) and Figure 5-19(a). This indicated that impedance measurements at much lower frequency of approximately 10^{-8} Hz was needed. This was not possible because of instrument limitation. Instead, the circuit model fits of the impedance data were used to the polarization resistances. The model was fitted to the impedance data using the mathematical approach detailed in Shukla [23].Circuit model fits to the partial mill-scale and mill-scale coupons' impedance data are shown in Figure 5-18(b) and Figure 5-19(b), respectively.

The fitted model was extrapolated up to 10^{-8} Hz for each coupon, and extrapolated impedance values are shown by solid lines in Figure 5-18(b) and Figure 5-19(b). As seen in the figures, the extrapolated impedance values attain steady-state at 10^{-8} Hz.

The impedance model fit parameters for each coupon are listed in Table 5-10. The constant phase element in the electrical circuit model contains parameters τ and α; the two parameters along with Rp are used to estimate effective double layer capacitance of the coupons' surface interfaces in contact with the test solution as per Equation 5.

$$C_{eff} = \frac{\tau^{\alpha}}{R_p A} \qquad \textbf{Equation 5}$$

where

C_{eff} — Effective double layer capacitance (F/cm2)
τ — Constant phase element time constant (**sec$^{\alpha}$**)
α — Constant phase element dimensionless parameter
R_p — Polarization resistance (Ω)
A — Electrode surface area (cm^2)

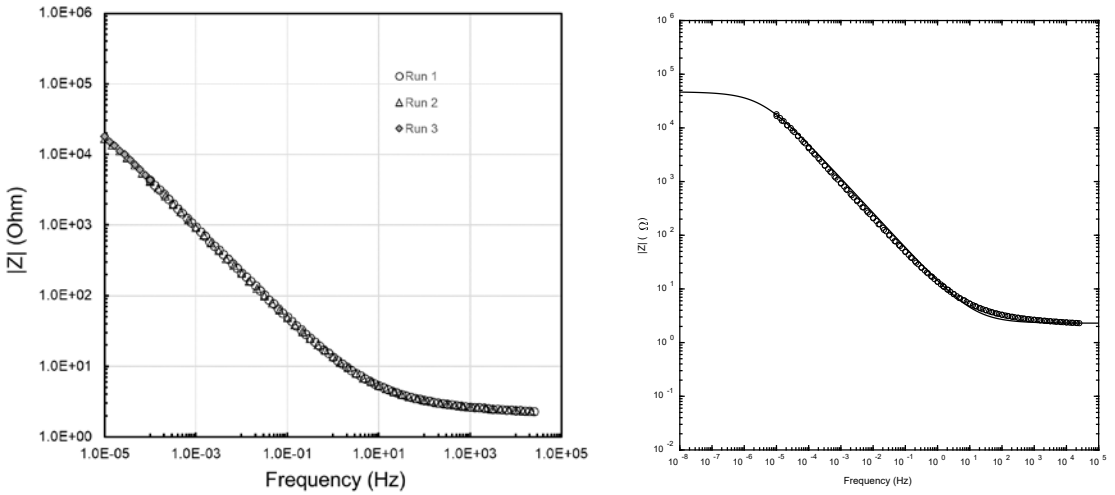

(a) EIS Data **(b) Circuit model fit to EIS data**

Figure 5-18 Bode Plot of Partial Mill-Scale Coupon (a) EIS Data and (b) Circuit Model Fit to EIS Data

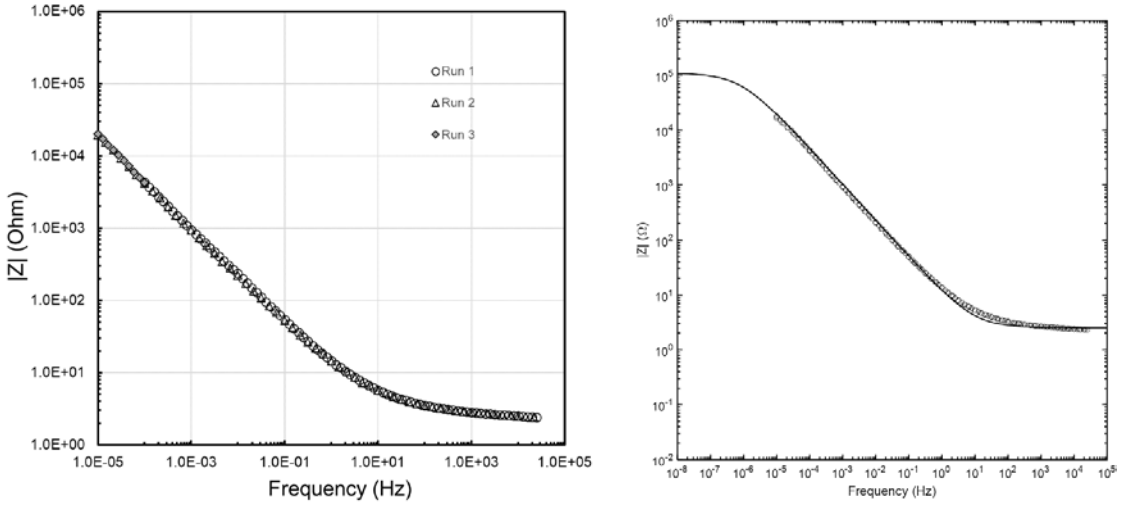

(a) EIS Data **(b) Circuit model fit to EIS data**

Figure 5-19 Bode Plot of Mill-Scale Coupon (a) EIS Data and (b) Circuit Model Fit to EIS Data

Table 5-10 Circuit Model Parameters Calculated using Model Fit to the Data

Parameter	Bullet Coupon	Partial Mill-Scale	Mill Scale
R_{sol} (Ω)	0.16	2.3	2.5
R_p (Ω)	1.245×10^5	4.7×10^4	1.12×10^5
α (unitless)	0.9	0.65	0.66
τ (sec^{α})	74.6	4.74×10^4	1.92×10^5
C_{eff} ($\mu F/cm^2$)	97.3	5820	6850

Rp of the three coupons are close to each other, but C_{eff} differ significantly. C_{eff} of partial and mill-scale coupons are two orders of magnitude higher than the bullet coupon.

CPP After OCP Hold: CPP measurements were conducted on the bullet and mill-scale coupons immediately after OCP hold. The CPP data is presented in Figure 5-20. The bullet coupon CPP data exhibited mixed response, similar to the data presented in Figure 5-12. The mill-scale CPP data exhibited negative hysteresis. The two coupons were extracted from the experimental setups and imaged. Image of the bullet coupon is presented in Figure 5-21(a). The coupon exhibited the same level of discoloration as seen in Figure 5-13 (a) and (c), however, no signs of pitting were visible. Images of the mill-scale coupon before and after the test are presented in Figure 5-21(b) and Figure 5-21(c); a comparison of the two images indicate no signs of pitting corrosion on the coupon surface. This observation is consistent with negative hysteresis response of the coupon surface.

CPP measurements were also conducted on the partial mill-scale coupon, but the measurement sequence was slightly different compared to the bullet and mill-scale coupons. The coupon was extracted from the experimental setup after OCP hold, surface examined, and placed back into the setup followed by CPP measurements. The CPP data for the partial mill-scale coupon is presented in Figure 5-22; CPP data for the mill-scale coupon is also presented in the figure for comparison. As seen in the figure, CPP data for the two coupons exhibit similarity; two CPP curves have negative hysteresis indicating no tendency of pitting corrosion for the coupons in the solution. Images of the partial mill-scale coupon before test, after OCP hold and after OCP hold plus CPP are presented in Figure 5-23 (a), (b), and (c), respectively. As seen in the figures, the coupon's images post OCP hold and OCP hold plus CPP are identical. In addition, no signs of pitting corrosion can be seen at the coupon surface following OCP hold and OCP hold plus CPP. Furthermore, coupon surface was not altered after OCP hold and OCP hold plus CPP. This observation is consistent with the negative hysteresis response of the coupon in the electrolyte.

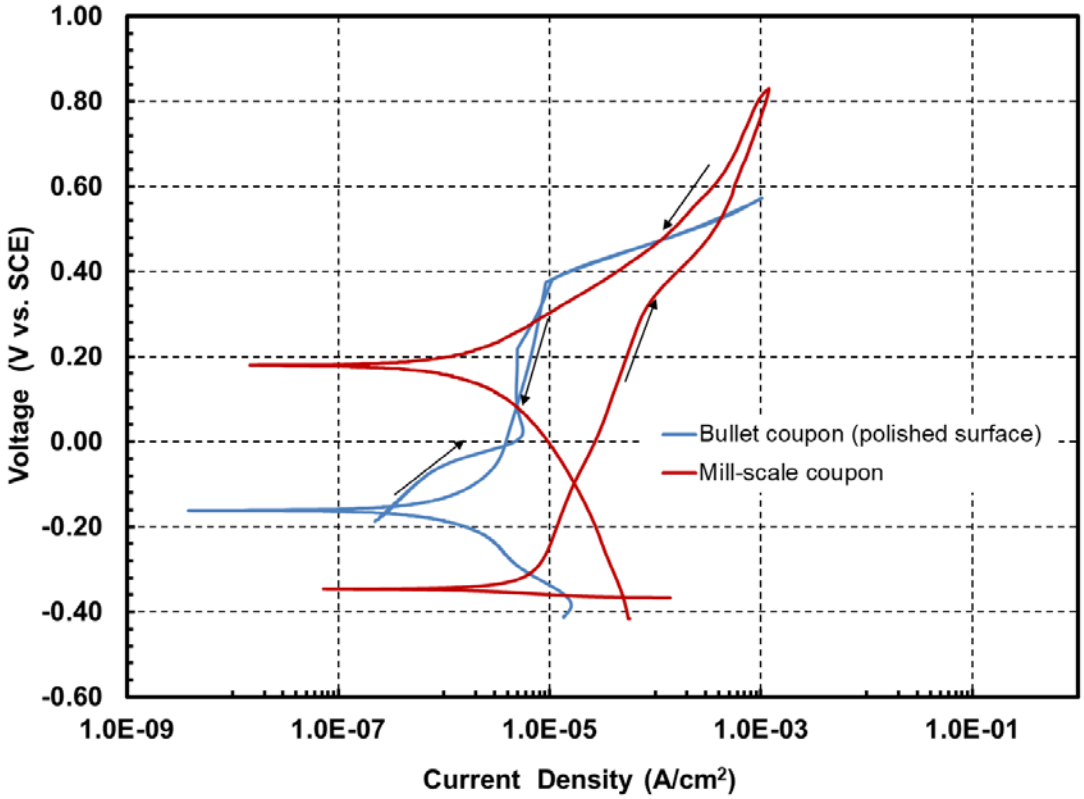

Figure 5-20 CPP Data after OCP hold

(a) Bullet coupon after OCP hold plus CPP

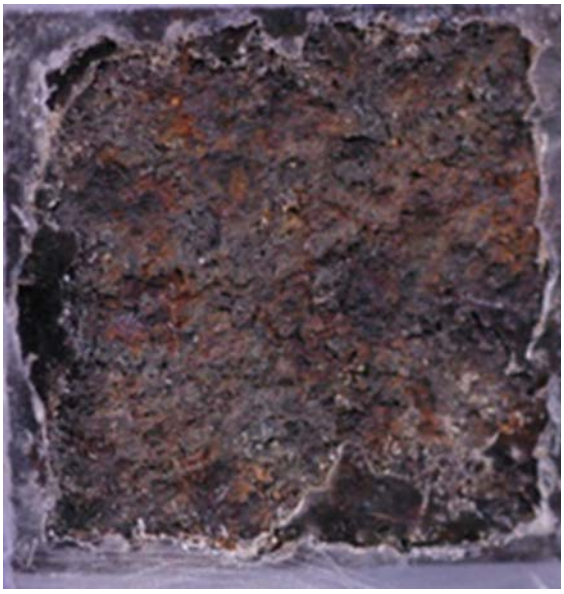

(b) Mill-Scale Coupons Before Test

(c) Mill-Scale Coupon after OCP hold plus CPP

Figure 5-21 Images of (a) Bullet coupon after OCP hold plus CPP, (b) Mill-Scale Coupons Before, and (c) Mill-Scale Coupon after OCP hold plus CPP

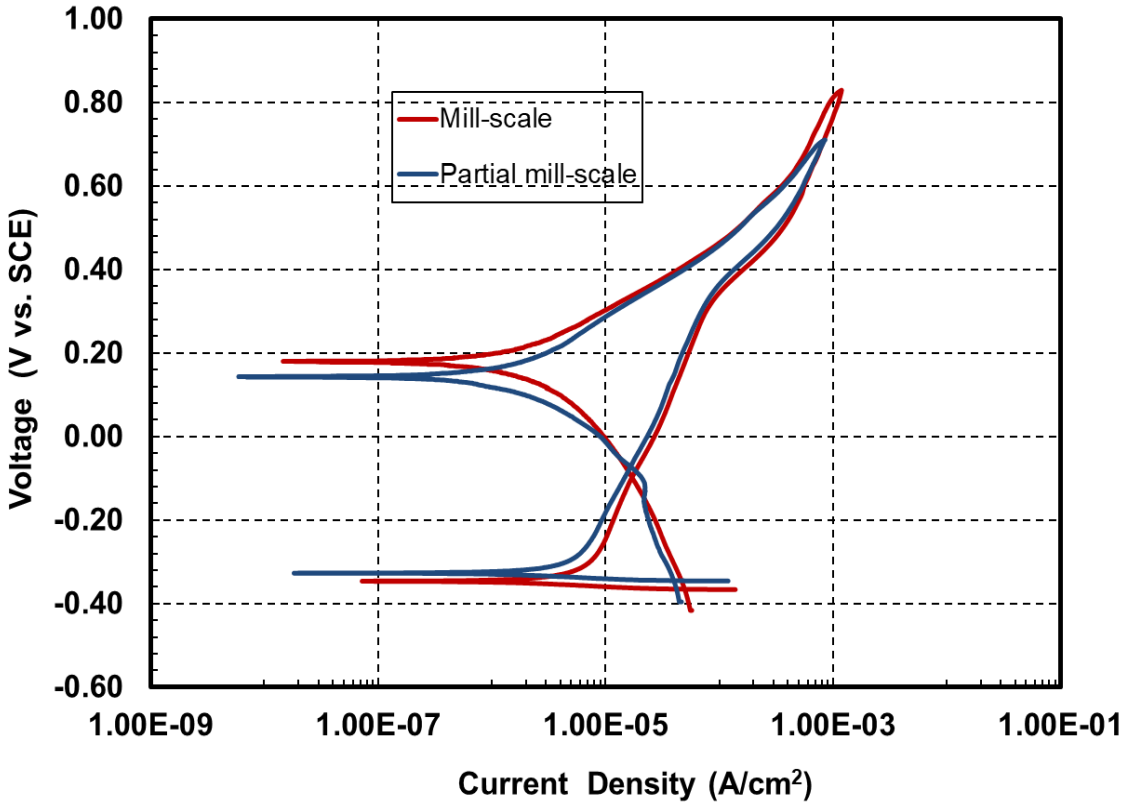

Figure 5-22 CPP Data of Partial Mill-Scale and Mill-Scale Coupons

(a) Before test **(b) After OCP hold** **(c) After OCP hold plus CPP**

Figure 5-23 Images of the partial mill-scale coupons (a) before test, (b) after OCP hold, and (c) after OCP hold plus CPP

Several prior studies have been reported with same type of carbon-steel in the high-level waste simulant environments which are comparable to these simulant chemistries. OCPs of U-bend coupons were recorded before measuring SCC susceptibility of the material [20],[22]. The OCP data was collected at 50 °C and is listed in Table 5-11. The OCP of all the samples became more noble or less negative over the course of the test, shifting between 80 to 207 mV more positive than

the initial OCPs. The largest shifts occurred for coupons in with 0.1 M OH^- and 0.1 M NO_2^- and without the indents. These coupons also had OCP values that were more anodic than coupons in the 0.01 M OH^- plus 0.01 M NO_2^- and with indents. The data also indicate some effect of surface condition on the OCP drift. For example, the terminal values in 8.5 M NO_3^- plus 0.1 M OH^- plus 0.1 M NO_2^- for as-received and heat-treated samples differed by 54 mV, indicating some effect of surface condition on the corrosion potentials.

Table 5-11 Open Circuit Potentials of U-bend Coupons [21, 22]

Solution Chemistry (M)			Surface Preparation*	OCP (mV_{SCE})	
$NaNO_3$	NaOH	$NaNO_2$		Initial	Final
5.5	0.01	0.01	AR, I	-332	-210
5.5	0.01	0.01	HT, I	-304	-216
8.5	0.01	0.01	AR, I	-309	-229
8.5	0.01	0.01	HT, I	-326	-221
8.5	0.1	0.1	AR, I	-305	-98
8.5	0.1	0.1	HT, I	-283	-152
8.5	0.01	0.01	AR	-312	-151
8.5	0.01	0.01	HT	-310	-128

* AR – as-received, HT – heat treated, I – indented

Another study on OCP evolution of A537 grade carbon steel in contact with AN-107 simulant was conducted [24]. The study included two different types of A537 steel: new A537 (A537 CL-1) and legacy/vintage A537 (A537 CL-2), with key difference being the surface condition between the new and vintage steel. The study test temperatures were 29 and 50 °C. The key difference between the current work and prior study was that the test solution and head space of the corrosion cells in the prior study were purged with Argon gas, thereby, removing any dissolved oxygen from the test solution. The OCP data were collected for 94 days. Initial and terminal OCP values are listed in Table 5-12.

Table 5-12 Open Circuit Potentials of new and vintage A537 steel in AN-107 simulant at 29 and 50 °C

Instance	OCP at 29 °C (mV_{SCE})		OCP at 50 °C (mV_{SCE})	
	New A537	Vintage A537	New A537	Vintage A537
Initial	-440 to -420	-440 to -420	-480 to -440	-440 to -420
Terminal	-440 to -420	-490 to -480	-450 to -440	~620

The data in Table 5-12 indicate that test temperature and surface condition play an important role in OCP evolution. The data also suggest that OCP evolution need not be anodic and could be cathodic in de-aerated solutions.

Sridhar et al. [24] reported OCP data for railroad tank car carbon steel in several high-level waste simulants. The coupons used in the study included ground surfaces. The authors reported that OCPs increased considerably over time, sometimes as much as 400 mV. The authors attributed this evolution to enhancement of the passive film on the surface, in terms of film thickness, chemistry, or electronic properties. The final potential correlated reasonably well with the initial solution pH measured at the test temperatures but did not correlate with any other parameters associated with chemistry of the test solution. The terminal OCP values in this work are consistent with data reported in Sridhar et al.

5.4 QEPAS Studies

5.4.1 *Calibration*

Procurement of the new sensor required the system to be recalibrated. In FY18 a manifold was automated to perform the calibrations using LabView. The data analysis was also automated using Octave. The process of a calibration is simple, gas is supplied to the QEPAS sensor by a mixing manifold where test gas (a certified ammonia cylinder) is diluted using clean dry nitrogen with mass flow controllers. In this way the concentration in the system can be stepped from 0 to the full concentration of the test gas as shown in Figure 5-24 (a), (b). In FY18 calibrations were performed over a wide range using two test gasses of 50 ppm ammonia in air and 550 ppm ammonia in air. The raw data is then reduced using an octave script to give measured concentration as a function of actual concentration as shown in Figure 5-24 (c), (d). The slope of this plot is the calibration factor in the QEPAS system.

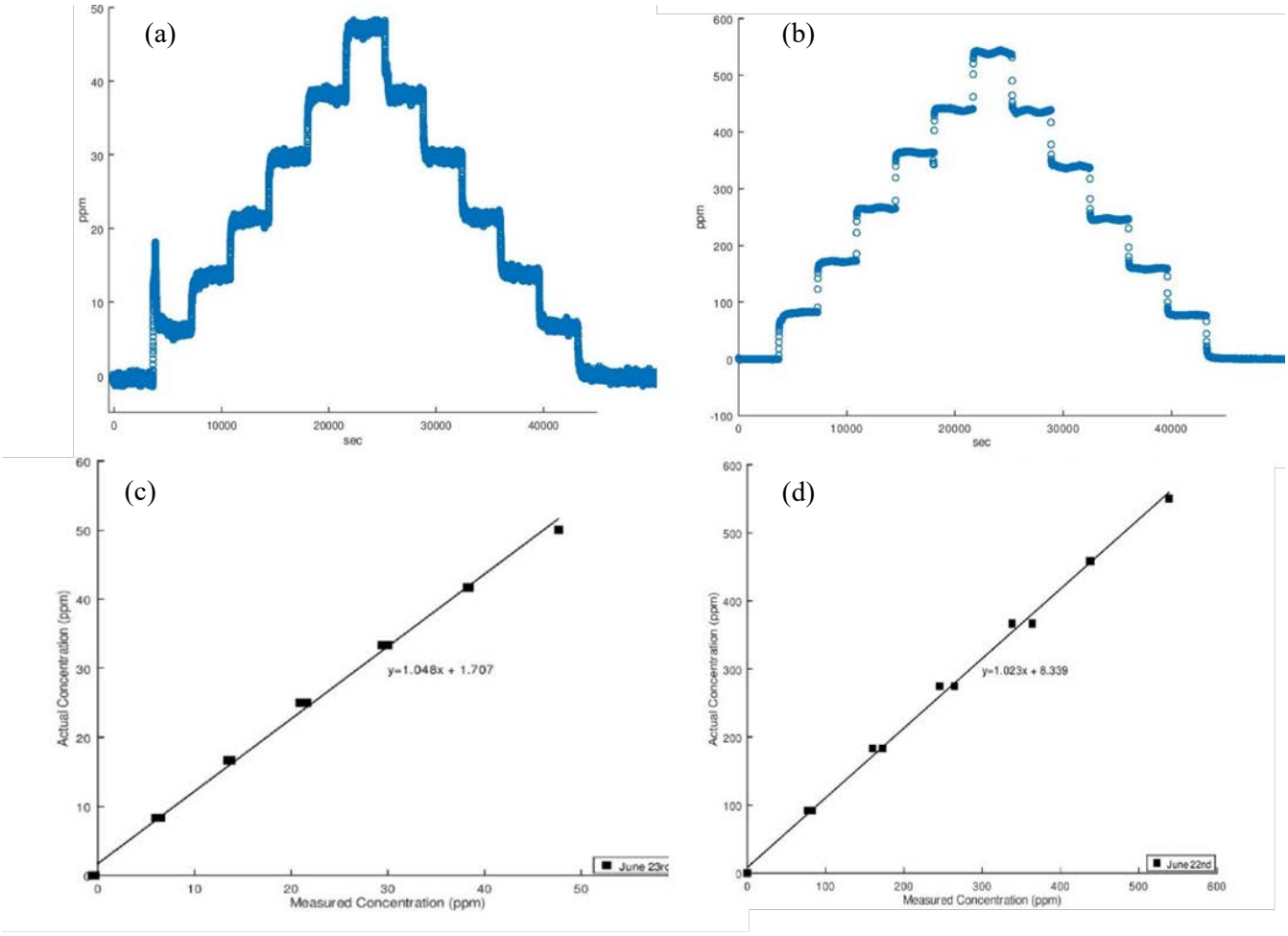

Figure 5-24 ADM calibration data, (a) 50 ppm ammonia raw calibration data, (b) 550 ppm ammonia raw calibration data, (c) measured vs actual concentration plot for 50 ppm ammonia test gas, and (d) measured vs actual concentration plot for 550 ppm ammonia test gas

5.4.2 *Humidity Tests*

To test the effect of water on the QEPAS system the calibration manifold was modified to allow for mixing test gas (ammonia in air) with humid nitrogen. Tests were run using the procedure described above for sensor calibrations. Figure 5-25 (a) shows the measured concentration as a function of time for one of the humidity tests. Figure 5-25 (b) shows the humidity as a function of time for the same test. Figure 5-25 (c), (d) show the reduced data for humidity tests using 50 ppm and 550 ppm test gas, respectively. As can be seen in the figure, the variation between the dry calibrations and the humid atmosphere tests is quite small, less than the instrumental uncertainty for the 50 ppm case and only slightly larger in the 550 ppm test.

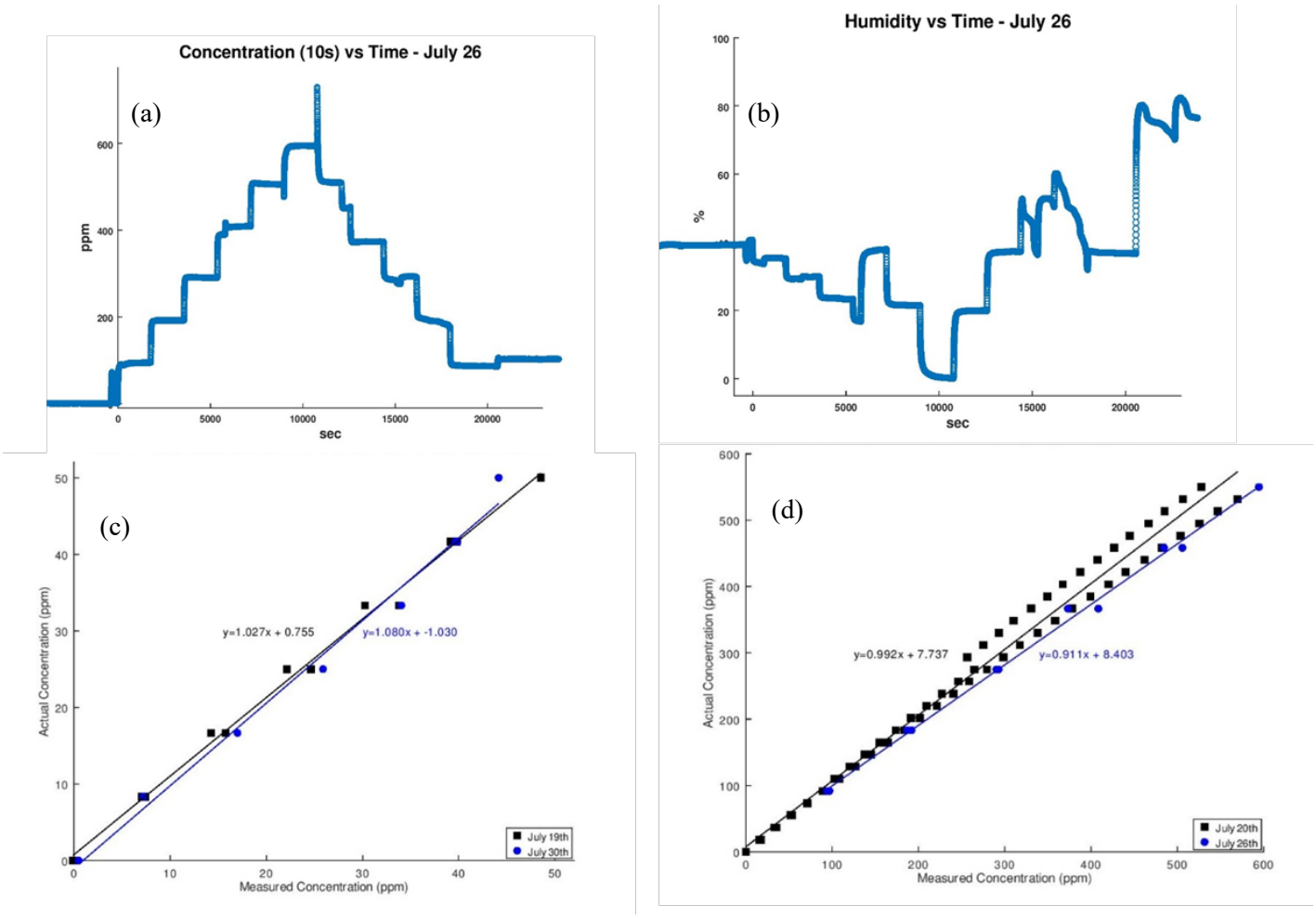

Figure 5-25 Humidity data collected using humidified nitrogen gas, (a) measured concentration using 550 ppm ammonia and nitrogen as humidified carrier gas, (b) measured humidity corresponding to the concentration values in figure a, (c) and (d) reduced concentration data showing actual vs measured ammonia concentration using 50 ppm and 550 ppm ammonia test gas, respectively.

5.4.3 *VSC Cell Tests*

After calibrating the new sensor and verifying that humidity effects are small in the concentration range of interest, the SRNL QEPAS system was connected to the exhaust of a VSC cell (Figure 5-26). The system was configured to simulate a VSC test with the QEPAS probe connected to the exhaust. Additionally, a 1/4" steel tube was added to the plumbing of the QEPAS sensor to allow for measurement of the NH_3 concentration in the cell as a function of height. It is important to remember that the QEPAS sensor is maintained at sub atmospheric pressures during operation. This causes a pressure gradient from the cell to the sensor which drives gas flow. Flow into the QEPAS sensor is controlled by a mass flow controller.

Figure 5-26 QEPAS system, gas control manifold, and VSC test setup, (A) electronics and laser housing, (B) QEPAS cell, housing the ADM, (C) gas control manifold, (D) gas input from ammonia cylinder, and (E) ammonia sampling probe for VSC measurements.

VSC tests are performed using very small flow rates when compared to the flows used in the initial QEPAS scoping studies. The flow rate used in VSC tests was 5-10 sccm, which leads to a very

large residence time for gas in the VSC cell, which has a volume of several liters. For this reason, it takes over 100 hours to fully replace the atmosphere in the VSC cell with the test gas and for measurements of the ammonia concentration in the cell to reach steady state. Figure 5-27 (a) shows the ammonia concentration in an empty VSC cell as a function of time. Additionally, to determine if low flow rate issues caused variations in concentration throughout the vessel, samples were collected at varying heights within the vessel. Initial testing began with the probe at the lower position, nearest the bottom of the vessel and additional data was collected at heights in the middle and top of the VSC vessel. Data shown in Figure 5-27 (b) indicates that there is a small detectable variance in concentration through the height of the vessel. This will be further studied during FY19. Upon completion of the initial height test, simulant VSC testing was conducted.

As shown in Figure 5-27 (c), the measured ammonia concentration in the vessel was significantly higher than the 50 ppm present in the test gas. This discrepancy can be attributed to the fact that the simulant solution was designed for a higher ammonia concentration. The test solution was optimized for ammonia concentrations of 550 ppm using ammonium nitrate as previously discussed. Figure 5-27 (d) shows the data for the beginning of the measurements and highlights two important details. First, the time to reach steady state ammonia concentration is relatively short when compared to the empty vessel, which suggests that the solution is the main contributor to the ammonia concentration in the headspace. Second, the jumps present every five hours are likely artifacts due to the internal system recalibration process. With that in mind, the uncertainty of the system over long time scales is largely dictated by the recalibration process, and therefore slightly larger than the ~5% uncertainty quoted for shorter runs. However, this uncertainty could likely be mitigated by optimizing the recalibration routine.

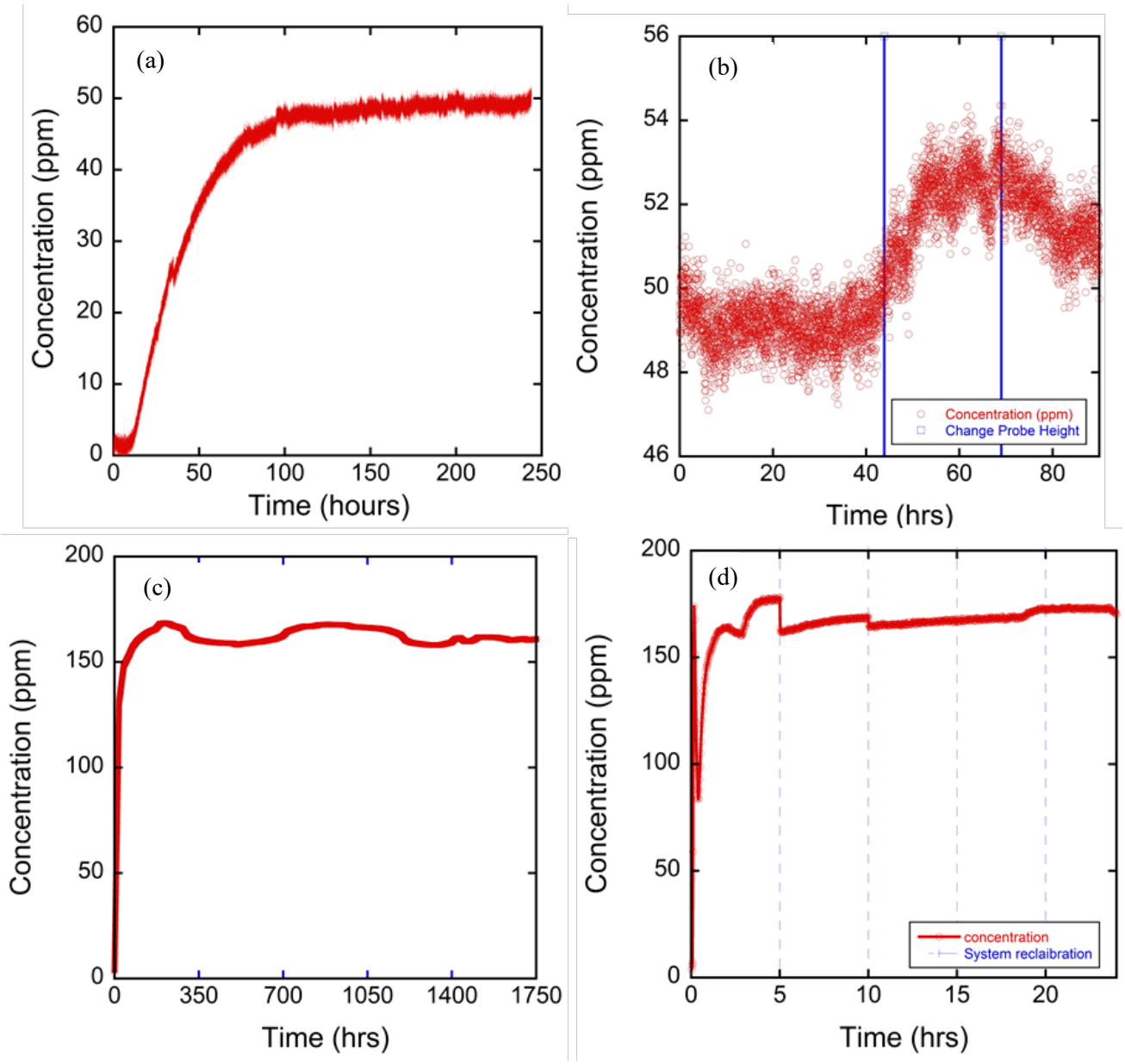

Figure 5-27 VSC vessel testing, (a) VSC concentration over time during an empty vessel test using 50ppm ammonia, (b) variance in ammonia concentration during probe height study, (c) VSC simulant test using 550 ppm ammonia simulant and 50 ppm ammonia gas, and (d) First 20 hours of VSC simulant with system recalibrations marked (blue line)

6.0 Conclusions

Conclusions of each task are provided for the FY18 corrosion studies supporting Hanford DSTs in several subsections on the next page.

6.1 New Limits

For the immersion tests, severe LAI corrosion was observed in three cases where the pitting factor was less than 0.5. Mitigation of LAI corrosion requires that the hydroxide concentration be maintained greater than 0.01 M and the pitting factor greater than 1.2.

Electrochemical testing in FY18, focused on pitting factors between 1 to 2 to target corrosion susceptibility for established borderline conditions and on fluoride effects to separate the halide coefficient in the pitting factor equation for fluoride and chloride contributions. The results on pitting factors between 1 and 2 were analyzed, and it seems that for pitting factors higher than 1, a pass is the most likely response with above 90% rate of success for the 15 tests performed. For the results of electrochemical testing to determine fluoride effects, it was determined that the contribution of chloride for the equation is around 3 times more significant than fluoride.

The pitting factor equation obtained was used to establish a waste chemistry envelope to minimize pitting corrosion for DSTs. The equation was validated with model simulations and comparison with historical results. The results were compiled in a memorandum that was submitted to WRPS summarizing the technical basis for the recommended changes in the chemistry controls. The resulting equation is presented below,

$$\text{Pitting Factor} = \frac{8.06\,[\text{OH-}]+1.55\,[\text{NO}_2\text{-}]}{[\text{NO}_3\text{-}]+16.7\,[\text{Cl-}]+5.7\,[\text{Fl-}]}$$

6.2 Secondary Liner Corrosion Studies

Vapor Space Corrosion and immersion tests with commercially available VCIs were performed on the rail-road car carbon steel samples at specific concentrations mixed with the groundwater simulant that has been pH adjusted to alkaline conditions. VCIs used for the study included:

- VpCI-645 + VpCI-609 solution with 10% VpCI-609 by weight of solution (100 g VpCI-609 in 1 liter) and 0.75% VpCI-645 by volume (7.5 mL/L), and

- VpCI-337 – 10% solution, i.e., 100 mL in VpCI-337 plus 900 mL of water for 1 L of the VCI solution

The VCIs were directly added to the groundwater solution at the start of the tests. The carbon steel coupons were immersed in the solution and, also, hanged in the vapor space of the corrosion cells. The study results indicated that both VCIs, i.e., VpCI-645 + VpCI-609 and VpCI-309, are effective in mitigating corrosion. However, one vapor space coupon in VpCI-337 environment exhibited pitting corrosion, but none in VpCI-645 + VpCI-609. This suggest that VpCI-645 + VpCI-609 combination is slightly more effective than VpCI-337 alone in mitigating corrosion, although more studies are needed to confirm. The issue of solid formation, i.e., precipitates, was investigated. The bottom precipitates in the test cells were due to formation of ferric hydroxide. GW simulant chemistry was prepared by adding ferric chloride and ferric sulphate. Addition of ferric chloride and ferric sulphate to water results in formation of ferric hydroxide which has very low solubility: this explains the bottom precipitates in the four figures. The floating precipitates in VCI-B was due to the VCI chemistry.

6.3 Anodic Drift Studies

Anodic drift experimental studies were conducted using AN-107 simulant and rail-road car steel coupons. Focus of the study was to determine effect of surface condition on OCP shift. AN-107 simulant was selected because pitting factor for the simulant was 1.66 which indicated uncertainty about the pitting corrosion tendency of the carbon steel. The study results showed that the drift could either be anodic or cathodic depending on the surface condition. For example, drift in corrosion potential was cathodic for the surface covered with mill-scale plus corrosion products, whereas the drift was anodic for an electrode with 600 grit ground surface. However, the terminal OCP values, i.e., OCP values at steady-state were independent of the surface conditions. CPP data collected after an OCP hold for 4 months indicated that pitting corrosion related electrochemical characteristics were not affected by the OCP evolution.

6.4 QEPAS studies

QEPAS was used to monitor the vapor space of a VSC test in FY18. Prior to configuring the system for this test, a new sensor was procured from Achray Photonics Inc. and several calibrations and tests were completed to confirm that the sensor was operational. These tests included: dry ammonia gas calibration at varying concentrations; humidity testing to verify that moderate fluctuations in humidity would not affect the QEPAS sensor during operation; and an empty VSC vessel test. The humidity testing indicated that there was no significant change in the error within the system for ammonia concentrations below 250 ppm (~5% error) and only a slight increase was detected for concentrations above 250 ppm (~9% error). During the empty vessel VSC testing, residence times of more than 100 hours were observed, which indicate that a solution containing a source of ammonia is required for vapor space simulations. Lastly, simulant VSC testing was conducted using the same vessel that was used during the empty vessel testing. These results indicate that there is significant contribution from the solution to the ammonia present in the system, and that utilizing an ammonium nitrate-based solution reduces the residence time of the vessel from >100 hours to <1 hour.

6.5 Recommendations

Recommendations for follow-on work are summarized below. These recommendations will be incorporated into a proposal for FY19 activities.

New Limits

- Assess interstitial liquid chemistry and temperatures and define additional testing needed.
- Identify any regions with less than adequate data coverage with the new testing protocol (e.g., pH 12-13).
- Prepare report that recommends operating envelope for DST waste chemistry.

Secondary Liner

- Address the formation of the precipitates in the bottom of the vessel. Consult with a vendor on alternatives VCI formulation.
- Perform the same test with pre-corroded samples to investigate the efficacy of the VCI with a more representative surface.
- Perform the same test with the VCI concentration at less than the vendor recommended dosage to investigate the efficacy at depleted VCI conditions.

Anodic Drift

- Utilizing corroded samples, perform the tests in simulated waste solutions over a broad range of pH (e.g., 10-14) and pitting factor (i.e., less than 1 to greater than 2). Ideally, the tests would evaluate potential pitting susceptibility (i.e., the red region) as well as the region where the risk of pitting susceptibility is less (i.e., the green region).

QEPAS

- Evaluate QEPAS capability for detection of other species. The detection of the VCI would be of particular interest as this may provide a means for in-situ detection of VCI depletion.
- Provide recommendations for field implementation of a QEPAS unit.

7.0 Quality Assurance

Data for all Tasks were recorded in the electronic laboratory notebook system, notebook number G8519-00126.

Requirements for performing reviews of technical reports and the extent of review are established in manual E7 2.60. SRNL documents the extent and type of review using the SRNL Technical Report Design Checklist contained in WSRC-IM-2002-00011, Rev. 2.

8.0 References

[1] P. K. Shukla, R. E. Fuentes, "SRNL Task Technical And Quality Assurance Plan for Hanford Double Shell Waste Tank Corrosion Studies-FY18", SRNL-RP-2018-00403, Savannah River National Laboratory, Aiken, SC, April 2018.

[2] L. M. Stock, J. R. Follett, and E. C. Shallman, "Specifications for the Minimization of the Stress Corrosion Cracking Threat in Double-Shell Tank Wastes," RPP-RPT-47337, Washington River Protection Solutions, Richland, WA, March 2011.

[3] T. Martin, "Outcomes from the August 2013 Expert Panel Oversight Committee Meeting," RPP-ASMT-56781, Washington River Protection Solutions LLC, Richland, WA, February 2014.

[4] R. E. Fuentes, "Hanford Double Shell Waste Tank Corrosion Studies-Final Report FY16", SRNL-STI-2016-00721, Savannah River National Laboratory, Aiken, February 2017.

[5] R. E. Fuentes, "Hanford Double Shell Waste Tank Corrosion Studies-Final Report FY17", SRNL-STI-2018-00116, Savannah River National Laboratory, Aiken, April 2018.

[6] A. Macias and M. L. Escudero, "The Effect of Fluoride Ion on Corrosion of Reinforcing Steel in Alkaline Solutions", Corrosion Science, Vol. 36, No. 12, p. 2169.

[7] R. E. Fuentes. B. J. Wiersma and K. Hicks, "Hanford Double Shell Waste Tank Corrosion Studies-Final Report FY14", SRNL-STI-2014-00616, Savannah River National Laboratory, Aiken, December 2014.

[8] R. E. Fuentes, R. B. Wyrwas, "Hanford Double Shell Waste Tank Corrosion Studies-Final Report FY15", SRNL-STI-2016-00117, Savannah River National Laboratory, Aiken, May 2016.

[9] B. Peters and D. Hitchcock, memo to B. Wiersma, SRNL-L4410-2017-0016, October 11, 2017.

[10] J. W. Congdon, "Evaluation of Corrosion Inhibitors for Washed Precipitate – Coupon Test Results," DPST-86-721, Savannah River Laboratory, Aiken SC, October 1986.
[11] R. P. Anantatmula, "DST Pitting Annual Report," WHC-SD-WM-PRS-016, Rev. 0, Westinghouse Hanford Company, Richland, WA, September 1996.
[12] R. Viola, N. Liberatore, D. Luciani and S. Mengali, "Quartz Enhanced Photoacoustic Spectroscopy for Detection of Improvised Explosive Devices and Precursors", Advances in Optical Technologies, vol. 2016, Article ID 5757361, 2016.
[13] ASTM A515, "Standard Specification for Pressure Vessel Plates, Carbon Steel, for Intermediate- and Higher-Temperature Service", ASTM International, West Conshohocken, PA, 2003.
[14] ASTM G1-03 "Standard Practice for Preparing, Cleaning, and Evaluating Corrosion Test Specimens", ASTM International, West Conshohocken, PA, 2011.
[15] ASTM G5-13 "Standard Reference Test Method for Making Potentiodynamic Anodic Polarization Measurements", ASTM International, West Conshohocken, PA, 2013.
[16] T. Martin, "Tank Integrity Expert Panel Corrosion Subgroup March 2016 Meeting Outcomes", RPP-ASMT-60833, Washington River Protection Solutions LLC, Richland, WA, May 2016.
[17] ASTM G192-08, "Standard Test Method for Determining the Crevice Repassivation Potential of Corrosion-Resistant Alloys Using a Potentiodynamic-Galvanostatic-Potentiostatic Technique", ASTM International, West Conshohocken, PA, 2014.
[18] S. Tsujikawa and Y. Hisamatsu, "On the repassivation potential for crevice corrosion" Corrosion Engineering, Japan, 29, 37, 1980.
[19] K. J. Evans, S. Chawla, K. M. Sherer, J. Gerst, J. Beavers, N. Sridhar and K. D. Boomer, "The Use of ASTM G192 to Evaluate the Susceptibility of Hanford Tank Steels to Pitting Corrosion", CORROSION/2016. Paper No. 51316-7688, NACE International, Houston, TX, 2016.
[20] B. J. Wiersma, R. E. Fuentes, and L. M. Stock, "Chemistry Envelope for Pitting and Stress Corrosion Cracking", SRNL-STI-2019-00217, Savannah River National Laboratory, Aiken, SC, in draft.
[21] K. M. Counts, B.J. Wiersma, J.I. Mickalonis, "Determination of Corrosion Inhibitor Criteria For Type III/IIIA Tanks During Salt Dissolution Operations – Interim Report," Savannah River National Laboratory, WSRC-STI-2007-00552, Aiken, SC, 2007.
[22] B. L. Garcia-Diaz, J.I. Mickalonis, B.J. Wiersma, "Determination of Corrosion Inhibitor Criteria For Type III/IIIA Tanks During Salt Dissolution Operations – Summary Document," Savannah River National Laboratory, SRNL-STI-2009-00600, Aiken, SC, 2009.
[23] P. K. Shukla, "Stationary Hemispherical Electrode Under Submerged Jet Impingement and Validation of the Measurement Model Concept for Impedance Spectroscopy", Ph.D. Dissertation, Gainesville, Florida: University of Florida, 2004.
[24] N. Sridhar, J.A. Beavers, B. Rollins, S. Chawla, K. Evans, and X. Li, "Stress Corrosion Cracking and Localized Corrosion of Carbon Steel in Nitrate Solutions." Corrosion, Vol. 27, No. 7, pp. 927-942, 2016.

9.0 Appendices

Appendix A
Chemical Composition of Simulants used in New Limits Long Term Immersion Corrosion Testing

Appendix B
Pictures of Partial and Complete Immersion Corrosion Samples from New Limits Task after Test

Appendix C
3-D Measuring Microscope Images selected coupons for analysis of New Limits Long Term Immersion Testing

Appendix D
Open Circuit Potential, pH and Temperature vs. Time plots for New Limits Long Term Immersion Testing

Appendix E
Chemical Composition of New Limits Task with pitting factors of 1 to 2 with Cyclic Potentiodynamic Results and Pictures after Test

Appendix F
Chemical Composition of New Limits Task for fluoride effects with Cyclic Potentiodynamic Results and Pictures after Test

Appendix G
Chemical Composition of Simulants used in Secondary Liner Corrosion Testing

Appendix H
Pictures of Secondary Liner Corrosion Testing Samples after Test